Neurobiology of Disease

Cnksr2 Loss in Mice Leads to Increased Neural Activity and Behavioral Phenotypes of Epilepsy-Aphasia Syndrome

Eda Erata,[1] Yudong Gao,[1] Alicia M. Purkey,[1] Erik J. Soderblom,[1,3] James O. McNamara,[2] and Scott H. Soderling[1,2]

[1]Department of Cell Biology, Duke University Medical School, Durham, North Carolina 27710, [2]Department of Neurobiology, Duke University Medical School, Durham, North Carolina 27710, and [3]Proteomics and Metabolomics Shared Resource, Duke Center for Genomic and Computational Biology, Duke University, Durham, North Carolina 27708

Epilepsy Aphasia Syndromes (EAS) are a spectrum of childhood epileptic, cognitive, and language disorders of unknown etiology. *CNKSR2* is a strong X-linked candidate gene implicated in EAS; however, there have been no studies of genetic models to dissect how its absence may lead to EAS. Here we develop a novel *Cnksr2* KO mouse line and show that male mice exhibit increased neural activity and have spontaneous electrographic seizures. *Cnksr2* KO mice also display significantly increased anxiety, impaired learning and memory, and a progressive and dramatic loss of ultrasonic vocalizations. We find that Cnksr2 is expressed in cortical, striatal, and cerebellar regions and is localized at both excitatory and inhibitory postsynapses. Proteomics analysis reveals Cnksr2 anchors key binding partners at synapses, and its loss results in significant alterations of the synaptic proteome, including proteins implicated in epilepsy disorders. Our results validate that loss of CNKSR2 leads to EAS and highlights the roles of Cnksr2 in synaptic organization and neuronal network activity.

Key words: **aphasia; Cnksr2; EEG; epilepsy; HiUGE; proteomics**

Significance Statement

Epilepsy Aphasia Syndromes (EAS) are at the severe end of a spectrum of cognitive-behavioral symptoms seen in childhood epilepsies, and they remain an inadequately understood disorder. The prognosis of EAS is frequently poor, and patients have life-long language and cognitive disturbances. Here we describe a genetic mouse model of EAS, based on the KO of the EAS risk gene *Cnksr2*. We show that these mice exhibit electrophysiological and behavioral phenotypes similar to those of patients, providing an important new model for future studies of EAS. We also provide insights into the molecular disturbances downstream of Cnksr2 loss by using *in vivo* quantitative proteomics tools.

Introduction

Idiopathic focal epilepsies of infancy and childhood are devastating disorders for which the etiologic understanding and treatments are both currently limited. These disorders are quite diverse, ranging from benign Rolandic epilepsy to highly disruptive epilepsy-aphasia syndrome (EAS) disorders. At the severe end of EAS are Landau-Kleffner syndrome and continuous spike and wave during slow-wave sleep syndrome (CSWS), which are characterized by clinical seizures, electrical status epilepticus during sleep, cognitive abnormalities, and progressive aphasia (Deonna, 1991; Tassinari et al., 2000; Nickels and Wirrell, 2008). Children with EAS are treated with antiseizure medications; however, these medications are usually not effective in treating cognitive symptoms, and the majority of the children are left with permanent cognitive and language difficulties.

The first gene mutations associated with EAS were identified in *GRIN2A*, which encodes for a subunit of the NMDAR (Carvill et al., 2013; Lesca et al., 2013). Interestingly, GRIN2A mutations account for 10%-20% of the patients in this spectrum, suggesting that other unknown gene mutations are involved in EAS pathogenesis (Lesca et al., 2013; Yang et al., 2018). While a mouse model for GRIN2A exists, this model has its limitations for modeling EAS; unlike patients who carry heterozygous mutations, heterozygous mice show only subtle phenotypes, and the model

Received Mar. 27, 2021; revised Sep. 2, 2021; accepted Sep. 10, 2021.

Author contributions: E.E., Y.G., A.M.P., E.J.S., and S.H.S. designed research; E.E., Y.G., A.M.P., and E.J.S. performed research; E.E., Y.G., and J.O.M. analyzed data; E.E. wrote the first draft of the paper; E.E., Y.G., A.M.P., J.O.M., and S.H.S. edited the paper; E.E. and S.H.S. wrote the paper.

S.H.S. and Y.G. have filed a patent application related to the HiUGE technology; the IP has been licensed to CasTag Biosciences. S.H.S. is a founder of CasTag Biosciences; Duke University as an institution holds equity in CasTag Biosciences. The remaining authors declare no competing financial interests.

This work was supported by National Institute of Mental Health Grant MH111684 to S.H.S.; and National Institute of Neurological Disorders and Stroke Grant NS097717 to J.O.M. We thank Fiona Porkka, Dr. Ramona Rodriguez, and Dr. William Christopher Wetsel (Duke Mouse Behavioral and Neuroendocrine Core Facility) for technical support and advice; Shataakshi Dube and Jamie Courtland for support on writing; Dr. Mohamad Abdul Mikati for advice on mouse EEGs; Dr. Valérie Mongrain for help on identifying vigilance states; and the rest of the S.H.S. laboratory members for helpful discussion.

Correspondence should be addressed to Scott H. Soderling at scott.soderling@duke.edu.

https://doi.org/10.1523/JNEUROSCI.0650-21.2021

does not capture the male predominance observed in EAS (Tsai et al., 2013; Salmi et al., 2019). Thus, there is a need for additional *in vivo* models that more fully recapitulate patient phenotypes to study the etiology of EAS.

Recently, loss-of-function mutations in *CNKSR2* (Connector enhancer of kinase suppressor of Ras 2) have been associated with EAS in humans (Houge et al., 2012; Hu et al., 2016; Damiano et al., 2017; Sun et al., 2018; Polla et al., 2019; Bonardi et al., 2020; Daoqi et al., 2020). In contrast to *GRIN2A*, *CNKSR2* is located on the X chromosome and thus fits the male predominance seen in this spectrum. The main clinical features of these *CNKSR2* mutations are attention deficit hyperactivity disorder (ADHD), intellectual disability, childhood epilepsy with CSWS, and acquired aphasia.

CNKSR2 encodes for the protein Cnksr2, which belongs to the CNK family of scaffold proteins, namely, Cnk1, Cnk2 (Cnksr2), and Cnk3. Each CNK homolog differs in its expression profiles. Cnk1 and Cnk3 are widely expressed in many tissues, whereas Cnksr2 expression is mostly restricted to the brain (Fritz and Radziwill, 2011). *Cnksr2* has two protein-coding isoforms *Cnksr2a* and *Cnksr2b*, which differ at the C-terminus. Within brain, the highest expression of Cnksr2 is in glutamatergic neurons followed by GABAergic neurons, and very little to none detected in glial cells (Zhang et al., 2014; Zeisel et al., 2015).

Scaffolding proteins lack enzymatic activity and instead act as signal processing hubs by facilitating interactions between signaling components to enable their spatiotemporal organization into protein complexes (Good et al., 2011). Early studies suggested that Cnksr2 likely serves as a scaffold for Rho and Ras small GTPase signaling cascades (Therrien et al., 1998; Lanigan et al., 2003; Bumeister et al., 2004). More recently, data from *in vitro* studies show that Cnksr2 interacts with regulators of the Rho-family GTPase pathway, such as Arhgap39 (Lim et al., 2014), and may also facilitate the localization of the regulatory kinase TNIK to the synapse (Zieger et al., 2020). Yet, the signaling cascades Cnksr2 may organize *in vivo* remain unknown. Of interest, Cnksr2 also has several domains consistent with its suggested role as a synaptic scaffold. These include sterile alpha motif (SAM), PSD-95, DLG, ZO-1/2 (PDZ) domain, proline-rich motif, PDZ binding motif, and a membrane-binding pleckstrin homology domain. Given this putative synaptic scaffolding role of Cnksr2, it is conceivable that disruptions in Cnksr2 could render several downstream pathways altered.

Despite the accumulating genetic evidence that the loss of *CNKSR2* is causal for EAS, there have been no *in vivo* studies of Cnksr2 to determine whether its loss models the human condition or how these mutations contribute to neurocognitive symptoms. In this study, we generate a new transgenic KO mouse model to examine the behavioral, electrophysiological, and molecular changes resulting from Cnksr2 loss in mice. We find that loss of Cnksr2 in mice results in phenotypes strikingly similar to those of human patients with alterations to the synaptic proteome linked to neurologic disorders, including epilepsy. We propose Cnksr2 KO mice as a model with construct and face validity for futures studies of EAS.

Materials and Methods

Animals. Conditional Cnksr2 KO animals were produced by homologous recombination at the Duke BAC Recombineering Core and the Duke Transgenic Core Facility. Briefly, a targeting construct was prepared by bacterial artificial chromosome recombineering, placing *LoxP* sites flanking the second coding exon, exon 2 of *Cnksr2*. There are two isoforms of *Cnksr2* (Cnksr2a and Cnksr2b) that result in two proteins that differ at the C-terminus. Importantly, this targeting strategy preserves the native start codon and deletes the constitutive exon 2; thus, both isoforms are abolished. Embryonic stem cells selected for neomycin resistance were screened for homologous recombination by PCR across the long and short targeting arms, using primers within and outside the targeting cassette. Next, positive animals were crossed with a FLP Deleter mouse (JAX #006054) line to remove the Neo cassette. Founder *Cnksr2* floxed mice were backcrossed with C57BL/6J WT (JAX #000664) animals 4 times. For behavioral testing and other studies, *Cnksr2* floxed mice were crossed with CMV-Cre (Schwenk et al., 1995) mice. Littermate WT ($Cnksr2^{+/Y}$) and hemizygous KO ($Cnksr2^{-/Y}$) males from heterozygous pairings were used in all experiments. For three-chamber sociability and adult ultrasonic vocalization (USV) behavioral tasks, C3H/HeJ female mice were purchased from The Jackson Laboratory (JAX #000659). All mice were housed in the Duke University's Division of Laboratory Animal Resources facilities, and all procedures were conducted with a protocol approved by the Duke University Institutional Animal Care and Use Committee in accordance with National Institutes of Health guidelines. Animals were transferred to the Duke Mouse Behavioral and Neuroendocrine Core Facility for behavioral testing.

RNA ISH assay. Single-plex RNAScope ISH was designed and implemented at Advanced Cell Diagnostics as previously published (Wang et al., 2012). The single-color probe for Cnksr2 (targets 1832-2803 nt of NM_177751.3) was predesigned and commercially available. RNA ISH was performed using the RNAscope 2.5 HD Red Reagent Kit (#322350) on 10 μm PFA-fixed brain sections of P0, P12, and P60 WT mice (2 animals per age group, 3 or 4 slices each). RNA quality was evaluated for each sample with a control probe specific to the housekeeping gene cyclophilin B (PPIB). In addition, negative control background staining was assessed using a probe specific to the bacterial *dapB* gene.

Multielectrode array (MEA). Postnatal day 0 neurons from WT or Cnksr2 KO cortex were plated in a 48-well MEA plate (Lumos 48, Axion Biosystems), and neuronal activity was recorded at day 6, 8, 10, and 12 d after plating (DIV). Each well contains a 4×4 grid of 50-nm-diameter electrodes with a pole-to-pole electrode spacing of 350 μm. Wells were coated with 1 mg/ml of poly-L-lysine in sodium borate buffer, pH 8.5. Neurons were plated at 120,000 cells/well spotted onto the electrode grid within the inner well. At 5 DIV, 5 μM of cytosine arabinoside was added and then fed every other day using basal media. Recordings of local field potentials were performed at 37°C with 5% CO_2 using a Maestro MEA system and AxIS software (Axion Biosystems). Ten minutes after the MEA plates were placed on the stage, 10 min recordings were used to calculate the metrics. Only wells that showed >12 active electrodes were included for further data analysis. Data were acquired at a rate of 12.5 kHz filtered with a digital Butterworth bandpass of 200-3000 Hz. The threshold for spike detection was fixed at 6× SD. Independent measurements were taken from triplicate MEA plates with 16-24 wells for each condition. Electrode bursting is defined as a minimum of 5 spikes separated by <100 ms between each spike. Representative raster plots were generated using Neural Metrics Tool (Axion Biosystems). Data were collected from three different MEA plates.

Animal surgery. $Cnksr2^{+/Y}$ and $Cnksr2^{-/Y}$ mice, at the age of P30-P35, were anesthetized with isoflurane (3% for induction and 1%-2% for maintenance). A 1.5 cm rostral-caudal incision in the skin was made to expose the skull surface. An EEG/EMG Mouse Headmount (Pinnacle Technologies, #8201) was aligned to the skull so that the front edge of the implant was 3-3.5 mm anterior to bregma and mounted using cyanoacrylate. Using 23-gauge needles, screw holes were created. Four miniature stainless-steel screws at the following coordinates (relative to bregma) were used as EEG electrodes: EEG2 (AP: 2 mm, ML:1.5 mm) (central), EEG1 (AP: −4 mm, ML: 1.5 mm) (occipital), ground (AP: 2 mm, ML: −1.5 mm), and reference (AP: −4 mm, ML −1.5 mm); 0.10 inch screws were used for anterior placement, and 0.12 inch screws were used for posterior placement. A two-part epoxy was applied between screw heads and the silver coating on the holes of the head implant. Screws were tightened until the screw heads rested on the board base. To insert the EMG wires, a small pocket in the nuchal muscles was made

using forceps. EMG wires were inserted into the opening. Dental cement was applied to insulate and protect the EEG leads.

EEG/EMG recordings and analysis. EEG/EMG recordings were initiated 7-14 d after surgery. Freely moving continuous EEG recordings were conducted for 1 or 2 separate sessions of 24 h per animal. The EEG recording apparatus (Pinnacle Technologies) consisted of a 100× preamplifier to record two EEG channels and 1 EMG channel. Simultaneous video recordings were collected using a night vision HD Digital Camera. Data were sampled at a rate of 500 Hz with 1.0 Hz high pass filtering and 45 Hz low pass filtering. EEG1, EEG2, and EMG signals were collected on Sirena Acquisition software (Pinnacle Technologies). Both EEG1 and EEG2 are differential recordings and share a common reference electrode. Epileptiform discharges of varying duration were detected using Seizure Pro software (Pinnacle Technologies). Spike wave complexes with a frequency of 2-10 Hz, voltage 2 times the background EEG, and a minimum duration of 1 s were included in the quantification of epileptiform discharges. To detect electrographic seizures, an automated line length search method was applied to all EEG channels with the threshold set at a length of 5000 per second using a 10 s search window and 1 s sliding window. High amplitude events with line length higher than 5000 per second, containing more than one spike-like event per second and persisting longer than 10 s were classified as electrographic seizures. Events detected by Seizure Pro software were confirmed or excluded by visual inspection of the EEGs and the video recordings. To identify periods of non-rapid eye movement sleep (NREMS), δ frequency (1-4 Hz) was extracted from FFT-transformed EEG data, visually inspected and manually scored. Based on δ power, three states were identified as wake/rapid eye movement sleep (REMS), NREMS, and transition periods between NREMS and wake/REMS.

Open field testing. Mice were placed into a square (21 cm × 21 cm) open field (AccuScan Instruments), and their motor activities were monitored for over 1 h under a 350 lux illumination using VersaMax software (AccuScan Instruments). AccuScan software scored the total distance traveled, vertical activity (beam-breaks), and time spent in the center zone.

Elevated zero maze. Mice were evaluated for anxiety-like behaviors using the elevated zero-maze. Mice were introduced into a closed portion of the maze and were given 5 min of free exploration under dim (40-60 lux) illumination. Activity was scored by Ethovision XT 7 (Noldus Information Technology) using a high-resolution camera suspended 180 cm above the center of the maze. Tracking profiles were generated by Ethovision XT software and were used to measure the percent time spent in the open areas and total number of transitions through open areas between the two closed quadrants.

Morris water maze. Spatial learning and memory were examined in the Morris water maze. All training and testing were conducted in a 120-cm-diameter stainless-steel pool filled with water, made opaque with white nontoxic poster paint and maintained at 24°C. The pool was divided into four quadrants: northeast (NE), northwest (NW), southeast (SE), and southwest (SW). Mice were acclimated to water for 5 d before testing. One day before testing, mice were trained to stand on the hidden platform in the NE quadrant for 20 s and then were allowed to swim freely for 60 s before being returned to the platform for 15 s. On the following day, water-maze testing started, with testing divided into two phases: acquisition (days 1-8) with the hidden platform in the NE quadrant and reversal (days 11-18) with the platform in the SW quadrant. Every day the mice received four trials in pairs that were separated by 60 min. Release points were randomized across test trials and test days. On days 2, 4, 6, 8, 12, 14, 16, and 18, a single probe trial was given 1 h after the four test trials. For probe trials the platform was removed from the water and the mice were released from the southernmost point on days 2, 4, 6, and 8 and from the northern-most point on days 12, 14, 16, and 18. Performance on all tests was video-recorded and scored with Ethovision XT 9 (Noldus Information Technology) according to swim time, swim distance, and swim velocity.

Y maze spontaneous alternation. Spontaneous alternation in a Y-maze was conducted under indirect illumination in a 3-arm Y-maze. For each trial, a mouse was placed into the center arm of the maze and permitted to freely explore for 5 min. All tests were recorded and scored subsequently by an observer who was blind to the genotypes of the mouse. Entry into an arm was defined as the mouse being >1 body length into that arm, with both hind-paws past the entrance to that arm. An arm alternation was defined as three successive entries into each of the different arms. Alternation, calculated as the total number of alternations divided by the total number of arm entries minus 2, was expressed as a percentage.

Novel object recognition. Testing was conducted on 3 consecutive days. On the first day, animals were acclimated to the arenas for 5 min. On the next day, mice were individually placed into test boxes and presented with two identical objects for 5 min. Mice were then returned to their home cage for 30 min before being returned to the test arena for a 5 min short-term memory retention test, where one training object was replaced with a novel object. The animals were reexamined 24 h later for long-term memory retention in a 5 min test with the familiar training object paired to a second novel object. All tests were filmed with digital cameras, and the videos were analyzed with Ethovision XT 7 software (Noldus Information Technology) that automatically tracked the location of each animal as well as the location and movement of the animal's head and nose during testing. Recognition scores were calculated by subtracting the time spent with the familiar object from the time spent with the novel object and dividing this difference by the total time spent with both objects.

Memory load testing. For memory load testing, mice were subjected to seven test trials in a large arena. On each trial, a new object of similar size was added successively to the other objects. On Trials 1-3, mice were allotted 3 min to explore the objects. On Trials 4 and 5, they were given 4 min; and on Trials 6 and 7, they were given 5 min. Testing started when the mouse was placed into the arena with the first object. At the end of trial, the mouse was removed to its home cage. The second object was added to the arena, and the mouse was returned to the test chamber. This was repeated for all trials. On each trial, the added object was termed the "target" object. All behaviors were videotaped, and Noldus Ethovision 11 and nose-point tracking were used. The duration of time spent with the target object and the mean time spent with the other objects were calculated from the tracking profiles for each trial. Preference index was calculated by subtracting the mean time spent with the other objects from the time spent with the target object, and dividing this difference by the total time spent with all objects.

Three-chamber sociability test. The three-chamber sociability test was performed as described by Kim et al. (2013). The test apparatus consisted of three chambers (54 × 26 × 24 cm) illuminated at 80-110 lux. This test was composed of two phases: nonsocial exploration and social affiliation testing. In the first phase, the test mouse was placed into the center chamber and two small empty wire-mesh cages were located in each of the adjoining chambers. The mouse was given full access to all three chambers for 10 min. Then the mouse was removed to its home cage and a C3H female "social stimulus" mouse was placed into one of the wire-mesh cages while the other remained empty. The C3H female mice are commonly used as social stimulus mice, as they provide mild social stimulation without provoking threatening or reactive behaviors from the social partners (Rodriguiz et al., 2011; Wang et al., 2016). For the second phase of testing, the test mouse was returned to the center chamber and given full access to the apparatus for 10 min. All behaviors were videotaped across both test phases and analyzed by the TopScan program (CleverSys). Contact with a nonsocial or social stimulus was defined as the mouse approaching the wire-mesh cage and its nose being within 4 cm of the cage.

Rotarod testing. Rotarod testing (Med-Associates) was used to evaluate sensorimotor function. On day 1, the latency of each mouse to fall during an increasing rotational speed was measured on four different trials (4 rpm to 40 rpm over 300 s). Trials were terminated when the mouse fell from the rod or at 300 s. On day 2, the rod was maintained at a steady speed of 28 rpm, and four trials were conducted in the same manner as on day 1.

Pup USVs. The USVs of neonates were examined during brief maternal separation on postnatal day 5. Individual pups were placed in a Styrofoam recording chamber. An externally polarized condenser

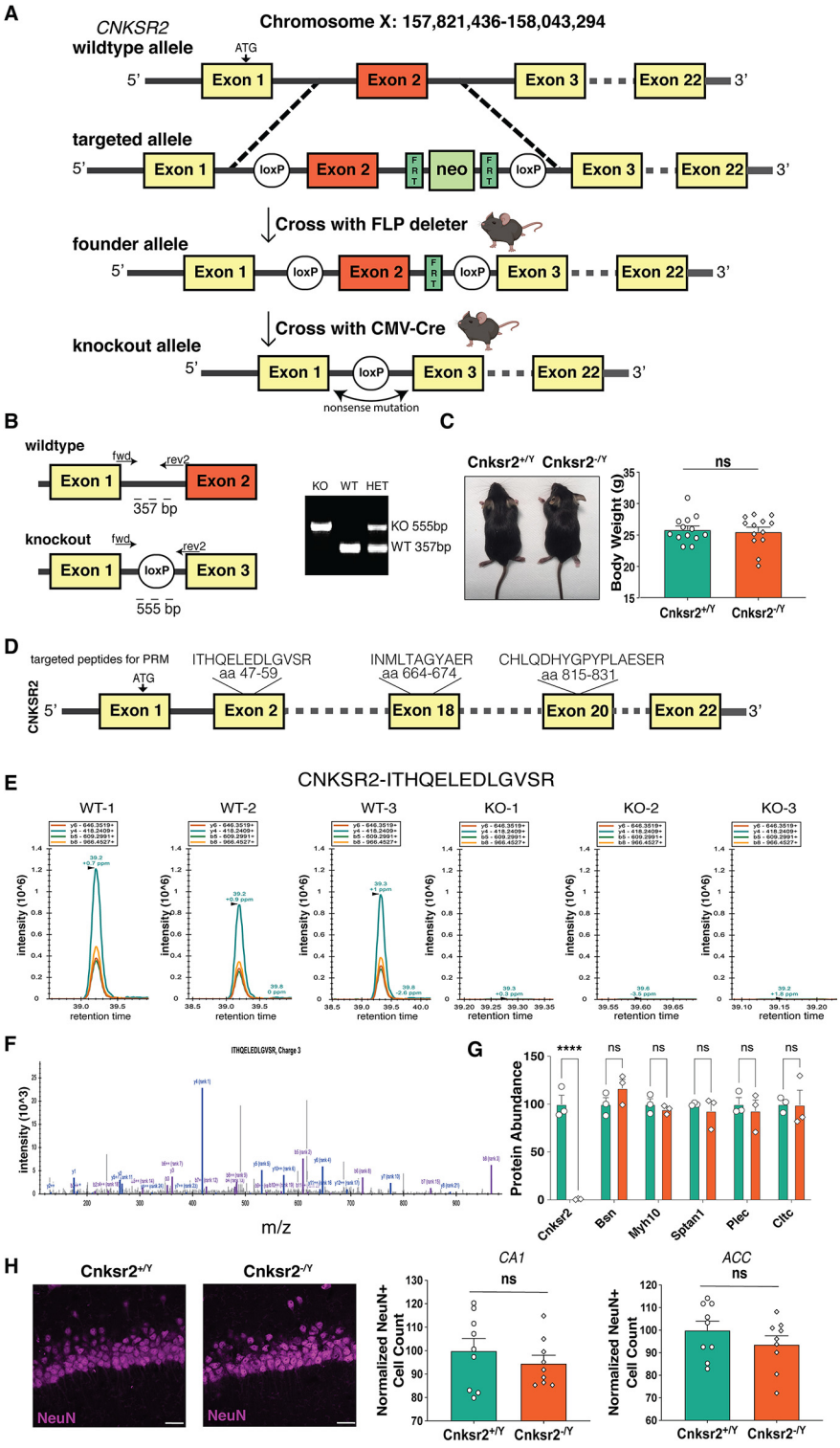

Figure 1. Generation of *Cnksr2*$^{-/Y}$ mice. ***A***, Schematic diagram of strategy to generate *Cnksr2*$^{-/Y}$ mice. A targeting vector was designed to disrupt the *Cnksr2* gene via homologous recombination in mouse embryonic stem cells, where two *loxP* sites were inserted upstream and downstream of exon 2. The resulting floxed line was crossed to FLP deleter line to remove the Neo cassette and establish germline transmission. Next, the founder line was crossed to CMV-Cre generate *Cnksr2*$^{-/Y}$ mice. ***B***, Left, Schematic of PCR strategy to detect WT and KO alleles. Arrows indicate primers used for detection. Right, Representative PCR genotyping results. ***C***, Left, Representative image of mice of each genotype. Right, Graphs of body weight of adult (P60-P75) *Cnksr2*$^{+/Y}$ and *Cnksr2*$^{-/Y}$ mice. ***D***, Schematic showing three different peptides targeted for PRM LC-MS assay to quantify Cnksr2 protein levels. ITHQELEDLGVSR is encoded by exon 2, INMLTAGYAER by exon 18, and CHLQDHYGPYPLAESER by exon 20. ***E***, Depletion of Cnksr2 in *Cnksr2*$^{-/Y}$ mice. PRM LC-MS assay to quantify relative protein expression levels across WT (left) and KO (right) animals. PRM chromatograms of the example ITHQELEDLGVSR peptide (m/z 499.5950 3+ precursor) for the four most abundant product ions from each mouse are shown. ***F***, Representative mass spectrum of ITHQELEDLGVSR following higher-energy collisional dissociation fragmentation. ***G***, Protein abundance of Cnksr2 and control proteins Bsn (Bassoon), Myh10 (Myosin-10), Sptan1 (Spectrin α chain), Plec (Plectin), and Cltc (Clathrin heavy chain 1) in *Cnksr2*$^{+/Y}$ and *Cnksr2*$^{-/Y}$ synaptosomes. Protein abundance was calculated by averaging the abundance of all three peptides targeted for all proteins. Cnksr2 protein was significantly depleted in Cnksr2 KO compared with the WT control. No differences were observed in control proteins: ****$p < 0.0001$ (two-way ANOVA with Bonferroni's multiple comparisons). $n = 3$ animals per group. Data were normalized by transforming the WT mean value into 100% and represent

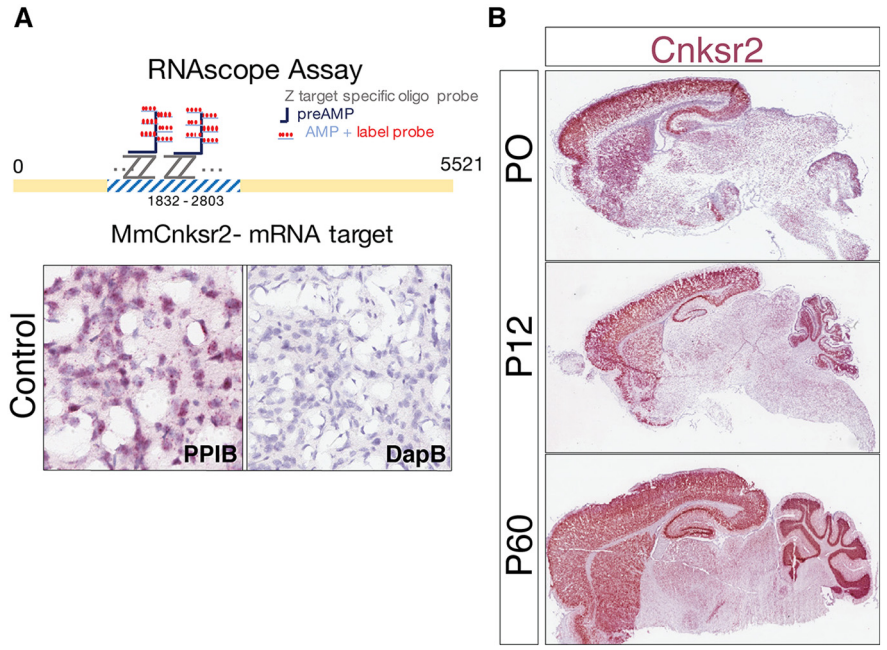

Figure 2. Expression of Cnksr2. ***A***, Top, RNAscope assay used to target and detect mouse Cnksr2 mRNA in the brain. Bottom, Control slices incubated with positive control probes (PPIB) and negative control (dapB). ***B***, Cnksr2 mRNA detection in sagittal sections (10 μm in thickness) from WT mice at ages P0, P12, and P30. Cnksr2 mRNA expression can be seen in cortex, hippocampus, striatum, and cerebellum. Scale bar, 1000 μm.

microphone was placed 15 cm above and pup USVs were recorded (10-200 kHz) for 90 s (Avisoft Bioacoustics). Spectrograms were analyzed with automated whistle tracking parameters (Avisoft SASLab Pro) and confirmed by hand-scoring. To avoid possible white-noise artifacts, frequencies outside the 25-120 kHz range were truncated and not included in the analyses. To avoid other ultrasonic artifacts, sounds <3 ms in duration were also excluded from the analysis.

Adult USVs. Animals were housed individually 1 week before testing. C3H/HeJ females were used as social partners. Males were primed twice with dirty bedding from female cages. Mice were acclimated to the recording chambers for 10-15 min a day before the testing. On the day of testing, C3H/HeJ females were visually inspected for estrus and females on estrus were used for the test. Test animals were placed into the test chamber for 2 min before the C3H female was introduced. Mice were allowed to explore the C3H stimulus for 8 min. Ultrasonic calls were recorded over the entire 10 min test as waveform audio files and analyzed subsequently using Avisoft SASLab Pro.

Homology-independent universal genome engineering (HiUGE)-mediated epitope tagging of endogenous Cnksr2. Primary cortical neuronal cultures, HiUGE targeting vectors, and small-scale adeno-associated viruses (AAVs) were prepared following a previously described method (Gao et al., 2019). Briefly, a gene-specific guide RNA (gRNA) vector was constructed targeting the genomic coding sequence near the C-terminus of mouse Cnksr2 (genomic target: ACTTCAGAAGAGATACTTAGTGG, terminal amino acids lost: 24 a.a.). It was paired with a HiUGE donor vector harboring the coding sequence of "spaghetti monster" smFP-V5 (a gift from Loren Looger, RRID: Addgene_59758) (Viswanathan et al., 2015) as the insertional payload to enable smFP-V5 labeling of Cnksr2 following endogenous expression. Donor vector paired with an empty-gRNA vector was used as a negative control. Small-scale AAV viruses (serotype 2/1) were produced in HEK293T cells, filtered through Spin-X filters (Costar, #8162), and applied to primary cortical neuronal cultures derived from $H11^{Cas9}$ mice (JAX, stock #028239) (Chiou et al., 2015) around DIV5. Cells were fixed with 4% PFA and 4% sucrose on DIV14, then blocked with blocking buffer (Abcam #ab126587, 1:10 in PBS with 0.3% Triton-X). Immunocytochemistry was performed by incubating in primary antibody overnight at 4°C, and in secondary antibody for 1 h at room temperature. Antibodies and dilutions: mouse anti-V5-epitope (Thermo Fisher Scientific, #R960-25, 1:500), rabbit anti-Homer1 (Synaptic Systems, #160002, 1:1000), guinea pig anti-Vglut1 (Synaptic Systems, #135304, 1:2000), guinea pig anti-Gephyrin (Synaptic Systems, #147318; 1:1000), guinea pig anti-VGAT (Synaptic Systems, #131004, 1:1000), goat anti-mouse AlexaFluor Plus 594 (Thermo Fisher Scientific, #A32742, 1:1000), donkey anti-rabbit AlexaFluor-647 (Thermo Fisher Scientific, #A31573, 1:1000), goat anti-guinea pig AlexaFluor-647 (Thermo Fisher Scientific, #A21450, 1:1000), goat anti-guinea pig AlexaFluor-488 (Thermo Fisher Scientific, #A11073, 1:1000), goat anti-rabbit AlexaFluor-488 (Thermo Fisher Scientific, #A11008, 1:1000), and goat anti-mouse AlexaFluor-647 (Jackson ImmunoResearch Laboratories, #115-605-166, 1:1000). Coverslips were counterstained with DAPI, mounted with FluorSave reagent (Millipore Sigma, #345789), and imaged on Zeiss 780 or Zeiss 710 confocal microscope (Carl Zeiss). The Puncta Analyzer plugin (Ippolito and Eroglu, 2010) on Fiji was used to count the number of colocalized puncta (Cnksr2-V5, Homer1 and Gephryin).

Genomic PCR detection of smFP-V5 integration at the Cnksr2 locus. Primary cortical culture of H11-Cas9 mice were transduced with small-scale AAV viruses (either Cnksr2-gRNA plus smFP-V5 donor, or smFP-V5 donor plus empty-gRNA as control) around DIV5, and harvested on DIV14. Genomic DNA was extracted using MyTaq Extract-PCR kit (Thomas Scientific, #C755G87), and nested PCR was performed using the following primer combinations to detect smFP-V5 integration: 1′ PCR, Cnksr2-Fwd′: GCCAGAGAAGGGGAAGTAGCC; and smFP-V5 Rev′:CCGTCGAGCTCAACCAGAATTG; 2′ PCR, Cnksr2-Fwd′: GG AAGCAGATGTACCTCGACC; and smFP-V5Rev′: CAGGCCCAACA GAGGGTTAG. Across junction PCR was also performed to detect the predominant WT band: Cnksr2-Fwd: GCCAGAGAAGGGGAAG TAGCC; and Cnksr2-Rev: TGAGTGTGTGTTAGAGAGGAAGTG.

Western blot detection of the Cnksr2-smFP-V5 fusion protein. Because Cnksr2 was labeled sparsely and expressed at endogenous levels, an immunoprecipitation enrichment strategy was used to detect the modified protein in low abundance. Neonatal H11-Cas9 pups received intracranial injections of purified AAV vectors (either Cnksr2-gRNA plus smFP-V5 donor, or smFP-V5 donor alone as control) between P0-P2 of age (4 mice per group). Two weeks following injection, mice were killed, and forebrain tissue was collected and lysed. Equal amounts of lysate were incubated with magnetic V5-trap beads (Chromotek, #v5tma-10) for 1 h at 4°C. After washes, bound protein was eluted with 2× Western sample buffer and subjected to SDS-PAGE. The membrane was probed for V5-epitope using rabbit anti-V5 antibody (Cell Signaling, #13202S, 1:1000), anti-rabbit HRP TrueBlot secondary (Rockland, #18-8816-31, 1:1000), and developed with Femto maximum sensitivity substrate (Thermo Fisher Scientific, #34094). Equal amount of input lysate was also subjected to SDS-PAGE, and the membrane was probed for GAPDH using rabbit anti-GAPDH (Abcam, #ab9485, 1:1000), and goat anti-rabbit 680CW secondary (LI-COR, #926-68071, 1:10,000).

←

mean ± SEM. See Extended Data Table 1-1. ***H***, Left, Representative images of NeuN (magenta) staining in $Cnksr2^{+/Y}$ and $Cnksr2^{-/Y}$ CA1 coronal slices. Scale bar, 20 μm. Right, Quantification of NeuN-positive cell numbers in CA1 and ACC reveals no significant differences in total the number of cells between genotypes. $p > 0.05$ (Student's t test). Three WT and 3 KO animals were used.

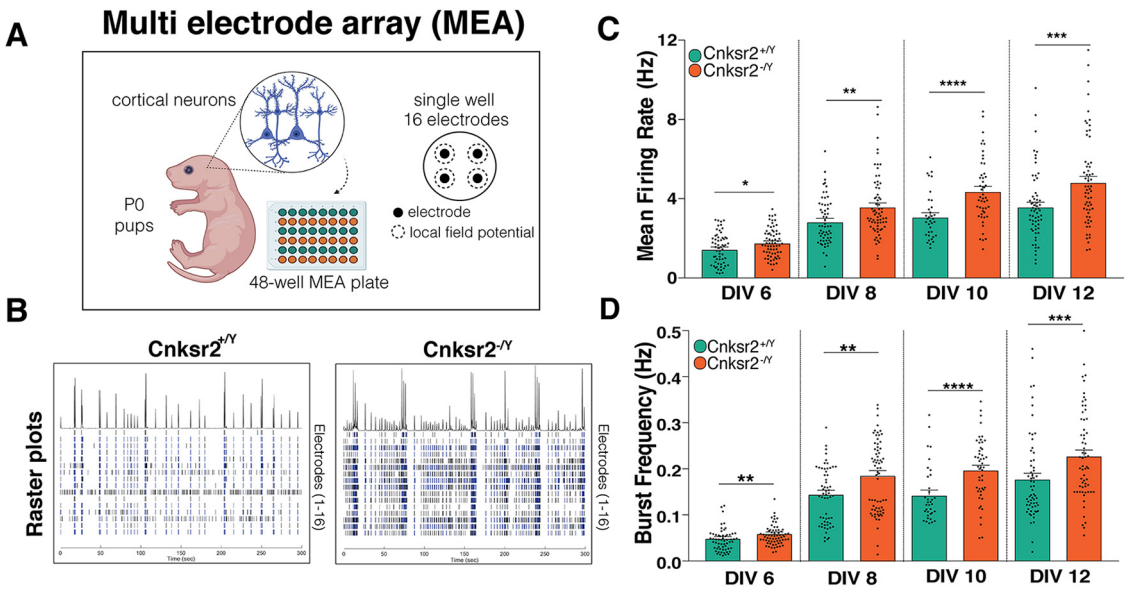

Figure 3. Cnksr2 loss leads to increased spontaneous firing and bursting rates of cortical neurons *in vitro*. ***A***, Experimental design to record spontaneous local neural activity using a MEA. Cultured cortical neurons were prepared from *Cnksr2*$^{+/Y}$ and *Cnksr2*$^{-/Y}$ neonatal pups at P0, and spontaneous neuronal activity was recorded at DIV6, DIV8, DIV10, and DIV12. Three *Cnksr2*$^{+/Y}$ and 3 *Cnksr2*$^{-/Y}$ mice were used for three MEA plates. Figure created with www.BioRender.com. ***B***, Representative raster plots showing spontaneous activity recorded from a *Cnksr2*$^{+/Y}$ (right) or *Cnksr2*$^{-/Y}$ (left) well on DIV8. ***C***, Graph of spontaneous mean firing rates. *Cnksr2*$^{-/Y}$ neurons displayed a significantly increased mean firing rate as early as DIV6 and up to DIV12 (DIV6: $*p = 0.02$; DIV8: $**p = 0.001$; DIV8: $****p < 0.0001$; DIV12: $***p = 0.0009$; Mann–Whitney test). $n = 3$ per genotype. ***D***, Graph of burst frequencies. Burst frequency in *Cnksr2*$^{-/Y}$ neurons compared with the WT control was also increased (DIV6: $**p = 0.0027$; DIV8: $**p = 0.0010$; DIV10: $****p < 0.0001$; DIV12: $***$ $p = 0.0008$; Mann–Whitney test). $n = 3$ per genotype. Data are mean ± SEM.

Synaptosome purification. *Cnksr2*$^{+/Y}$ and *Cnksr2*$^{-/Y}$ animals deeply anesthetized with isoflurane were decapitated, and their hippocampi were rapidly dissected and flash frozen. Next, synaptosomes were isolated biochemically from hippocampal tissue (26-30 mg). All steps for synaptosome isolation and purification were performed at 4°C. Tissue was homogenized on ice using homogenization buffer (1 ml, 320 mM sucrose, 5 mM HEPES, pH 7.4, 1 mM EGTA). The homogenate was centrifuged for 10 min at 1000 × *g*, and then the supernatant was transferred to a new tube and centrifuged for 20 min at 12,000 × *g*. The supernatant was removed, and the remaining pellet (crude synaptosomal fraction) was resuspended in resuspension buffer (400 μl, 320 mM sucrose, 5 mM Tris/HCl, pH 8.1). A discontinuous sucrose gradient was prepared, and the resuspended pellet was layered over a 0.8-1.0-1.2 M HEPES buffered sucrose gradient in a Beckman Ultra-Clear tube (catalog #344059). Next, tubes were centrifuged for 2 h at 85,000 × *g* in an ultracentrifuge. The synaptosomal plasma membrane fraction at the 1.0 M/1.2 M interface (~2 ml) was removed and layered over 0.8 M sucrose/HEPES in a fresh Ultra-Clear tube and centrifuged for an additional hour at 85,000 × *g*. The supernatant was discarded, and the remaining synaptosome pellet was frozen at −80°C. All buffers used were treated with protease inhibitors.

Parallel reaction monitoring (PRM) targeted proteomics. For the PRM analysis, 28 μg of total protein from synaptosome samples was used. Synaptosome samples were supplemented with SDS to a final concentration of 5% for digestion. Samples were then reduced with 10 mM dithiothreitol for 30 min at 80°C and alkylated with 20 mM iodoacetamide for 30 min at room temperature. Next, they were supplemented with a final concentration of 1.2% phosphoric acid and 1440 μl of S-Trap (Protifi) binding buffer (90% MeOH/100 mM TEAB). Proteins were trapped on the S-Trap, digested using 20 ng/μl sequencing grade trypsin (Promega) for 1 h at 47°C, and eluted using 50 mM TEAB, followed by 0.2% FA, and lastly using 50% acetonitrile (ACN)/0.2% FA. All samples were then lyophilized to dryness and resuspended in 15 μl 1%TFA/2% ACN containing 12.5 fmol/μl yeast alcohol dehydrogenase (ADH_YEAST). A Sampe Pool QC (SPQC) was created by taking 5 μl from each sample, which was run periodically throughout the acquisition period.

Quantitative LC-MS/MS was performed on 2 μl (1 μg) of the SPQC sample using a nanoAcquity UPLC system (Waters) coupled to a Thermo Orbitrap Fusion Lumos high-resolution accurate mass tandem mass spectrometer (Thermo Fisher Scientific) via a nanoelectrospray ionization source. Briefly, the sample was first trapped on a Symmetry C18 20 mm × 180 μm trapping column (5 μl/min at 99.9/0.1 v/v water/ACN), after which the analytical separation was performed using a 1.8 μm Acquity HSS T3 C18 75 μm × 250 mm column (Waters) with a 90 min linear gradient of 5%-30% ACN with 0.1% formic acid at a flow rate of 400 nl/min with a column temperature of 55°C. To create PRM assays, data were first collected on the Fusion Lumos mass spectrometer in a data-dependent acquisition (DDA) mode of acquisition with an $r = 120{,}000$ (at m/z 200) full MS scan from m/z 375-1500 with a target AGC value of 4e5 ions. MS/MS scans were acquired at Rapid scan rate (Ion Trap) with an AGC target of 1e4 ions and a maximum injection time of 100 ms. Up to three peptides from each protein of interest were selected from that DDA data to create the PRM assay. For PRM targeted runs, data were collected on the Fusion Lumos mass spectrometer in a PRM mode of acquisition with (1) an $r = 60{,}000$ (at m/z 200) full MS scan from m/z 375-200 with a target AGC value of 4e5 ions and (2) $r = 30{,}000$ (at m/z 200) MS/MS from m/z 300-2000 with a target AGC of 1e4 of target precursors (±5 ppm mass error) with a 1.2 Da isolation window. The peptides were scheduled by room temperature (RT) into 2 min windows. The duty cycle with this scan rate and scheduling resulted in a datapoint being collected every 1 s.

Following LC-PRM analyses, data were imported into Skyline (MacCoss Lab, University of Washington) for manual curation of peak integration and removing any potential interfering transitions. To assist with peak identification, DDA runs searched using the Mascot Database against a SwissProt Mouse database (trypsin enzyme rules, 5 ppm precursor and 0.8 Da product mass accuracy, curated at a 1% false discovery rate) were imported, and their identification times were overlaid onto the PRM traces. Data were then exported at the MS2 (fragment ion) level and included extraction of four fragment ions. For proteins that contained multiple peptides, the signal from each of the peptides was summed to create a protein level intensity. In addition to Cnksr2, PRM data were also acquired for five additional normalizing proteins (Myosin-10, Bassoon, Clathrin heavy chain 1, Plectin, Spectrin α chain) not expected to be differentially expressed across the different samples. This was accomplished by calculating the normalizing factors needed to

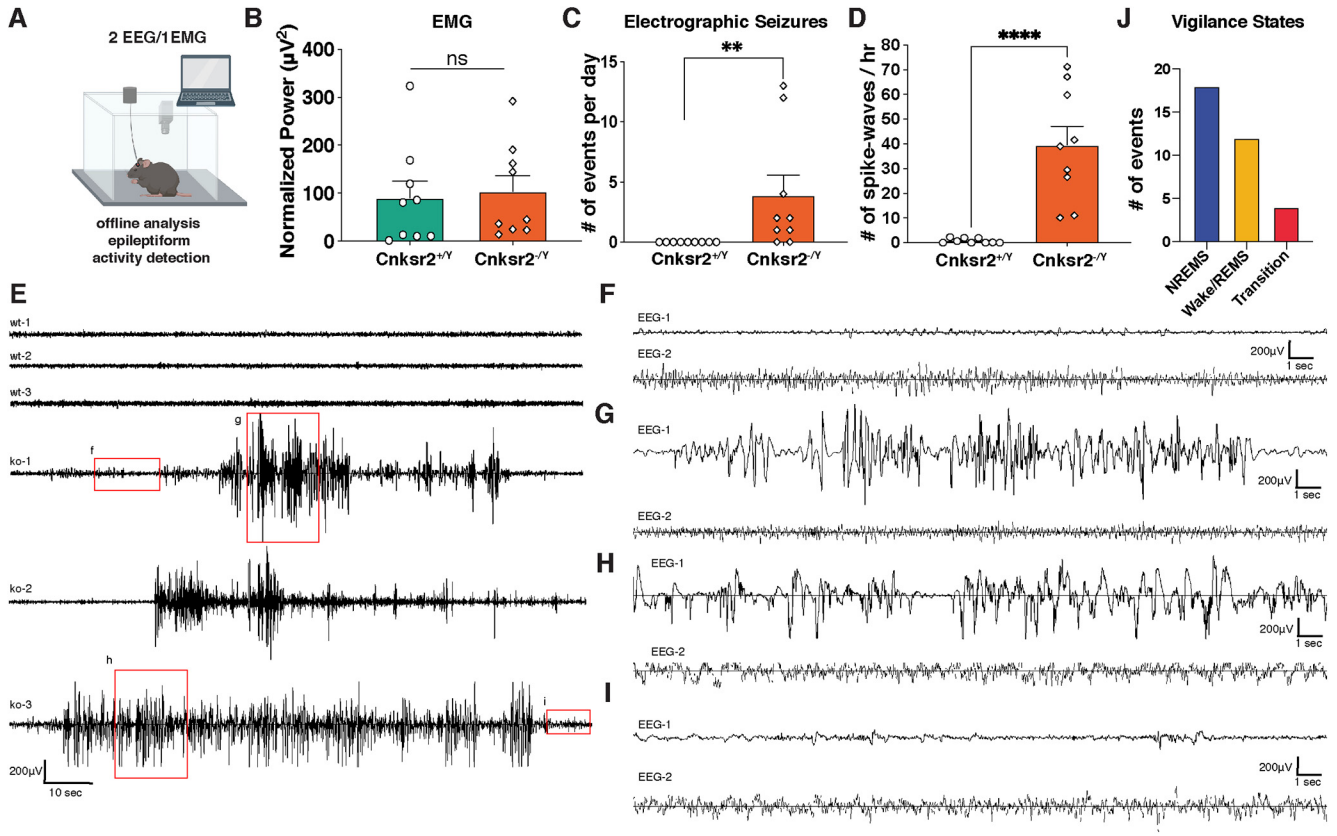

Figure 4. *Cnksr2*$^{-/Y}$ mice exhibit abnormal EEGs with epileptiform discharges. For handling-induced tonic-clonic seizure example, see also Movie 1. ***A***, Schematic of 2 EEG/1 EMG recording area for freely moving mice. ***B***, Graph of EMG full-spectrum power. No significant difference in average EMG power between genotypes was observed ($p > 0.05$; unpaired *t* test). Data were normalized by transforming the WT mean value into 100% and represent mean ± SEM. ***C***, Number of electrographic seizure events detected per day plotted for *Cnksr2*$^{+/Y}$ and *Cnksr2*$^{-/Y}$ mice. Five WT and 5 KO mice were used for the recordings, and each mouse was recorded for 1 or 2 sessions. A total of 35 events were detected in 5 KO (7 of 9 sessions) mice, and 0 events were detected in 5 WT mice (0 of 9 sessions). $^{**}p = 0.0011$ (Fisher's exact test, one-tailed). ***D***, Number of spike-wave discharges per hour quantified for *Cnksr2*$^{+/Y}$ and *Cnksr2*$^{-/Y}$ mice. Spike-wave complexes lasting >1 s and separated by <0.5 s were quantified and reported. Number of spike-wave complexes seen in EEGs were significantly increased in *Cnksr2*$^{-/Y}$ mice. $^{****}p < 0.0001$ (Mann–Whitney test). ***E***, Representative EEG1 traces. Top, WT baseline EEGs. Bottom, Traces of electrographic seizures detected in KO mice. ***F***, Baseline EEG-1 and EEG-2 electrode traces for ko-1 before the detected event. ***G***, Electrographic seizures detected in EEG-1 for ko-1. ***H***, Electrographic seizures detected in EEG-1 for ko-3. ***I***, Baseline EEG-1 and EEG-2 electrode traces for ko-3 after the detected event. ***J***, Identification of vigilance states in which electrographic seizure events occur in *Cnksr2*$^{-/Y}$ mouse. Nineteen events during NREMS, 12 events during awake/REMS, and 4 events during transition state between awake/REMS and NREMS were identified.

bring sample control protein value up to the average of all of the sample control protein values and then applying that correction factor to all of the individual sample proteins based on the levels of the control proteins. Results of PRM data can be found in (Extended Data Table 1-1).

Tandem mass tag (TMT) labeling and LC-MS/MS analysis. Synaptosome samples were supplemented with 100 μl of 8 M urea and probe sonicated. Protein concentrations were determined via Bradford Assay and ranged from 2.72 to 7.23 mg/ml. Samples were normalized to 100 μg using 8 M urea and spiked with undigested bovine casein at a total of either 1 or 2 pmol as an internal quality control standard. For the labeling and the fractionation, 40 μg of total protein was used. Next, they were supplemented with 13.9 μl of 20% SDS, reduced with 10 mM dithiothreitol for 45 min at 32°C, alkylated with 20 mM iodoacetamide for 45 min at room temperature, then supplemented with a final concentration of 1.2% phosphoric acid and 542 μl of S-Trap (Protifi) binding buffer (90% MeOH/100 mM TEAB). Proteins were trapped on the S-Trap micro cartridge, digested using 100 ng/μl sequencing grade trypsin (Promega) for 1 h at 47°C, and eluted using 50 mM TEAB, followed by 0.2% FA, and lastly using 50% ACN/0.2% FA. All samples were then lyophilized to dryness.

Each sample was resuspended in 200 μl 200 mM triethylammonium bicarbonate, pH 8.0 (TEAB); 100 μl was taken of each sample, and the remaining was combined to form an SPQC pooled sample. Fresh TMT11plex reagents (0.8 mg for each 11-plex reagent) were resuspended in 41 μl 100% CAN, and half was added to each sample. Samples were incubated for 1 h at room temperature. After 1 h reaction, 5 μl of 5% hydroxylamine was added and incubated for 15 min at room temperature to quench the reaction. Samples were combined within their respective sets then lyophilized to dryness.

Each set of samples were resuspended in 300 μl 0.1% formic acid; 400 μg was fractionated into 48 unique high pH reversed-phase fractions using pH 9.0 20 mM ammonium formate as mobile phase A and neat ACN as mobile phase B. The column used was a 2.1 mm × 50 mm XBridge C18 (Waters), and fractionation was performed on an Agilent 1100 HPLC with G1364C fraction collector. Throughout the method, the flow rate was 0.4 ml/min and the column temperature was 55°C. The gradient method was set as follows: 0 min, 3% B; 1 min, 7% B; 50 min, 50% B; 51 min, 90% B; 55 min, 90% B; 56 min, 3% B; 70 min, 3% B. Forty-eight fractions were collected in equal time segments from 0 to 52 min, then concatenated into 12 unique samples using every 12th fraction. For instance, fraction 1, 13, 25, and 37 were combined, fraction 2, 14, 26, and 38 were combined, etc. Fractions were frozen and lyophilized overnight. Samples were resuspended in 50 μl 1%TFA/2% ACN before LC-MS analysis.

Quantitative LC-MS/MS was performed on 2 μl (1 μg) of each sample, using a nanoAcquity UPLC system (Waters) coupled to a Thermo Orbitrap Fusion Lumos high-resolution accurate mass tandem mass spectrometer (Thermo Fisher Scientific) equipped with a FAIMSPro device via a nanoelectrospray ionization source. Briefly, the sample was first trapped on a Symmetry C18 20 mm × 180 μm trapping column (5 μl/min at 99.9/0.1 v/v water/ACN), after which the analytical separation was performed using a 1.8 μm Acquity HSS T3 C18 75 μm × 250

Movie 1. Example video showing tonic-clonic seizure in Cnksr2 KO mouse during cage change. [View online]

mm column (Waters) with a 90 min linear gradient of 5%-30% ACN with 0.1% formic acid at a flow rate of 400 nl/min with a column temperature of 55°C. Data collection on the Fusion Lumos mass spectrometer was performed for three difference compensation voltages (−40, −60, −80 V). Within each CV, a DDA mode of acquisition with an $r = 120{,}000$ (at m/z 200) full MS scan from m/z 375-1600 with a target AGC value of 4e5 ions was performed. MS/MS scans were acquired in the Orbitrap at $r = 50{,}000$ (at m/z 200) from m/z 100 with a target AGC value of 1e5 and maximum fill time of 105 ms. The total cycle time for each CV was 1 s, with total cycle times of 3 s between like full MS scans. A 45 s dynamic exclusion was used to increase the depth of coverage. The total analysis cycle time for each sample injection was ~2 h.

Following UPLC-MS/MS analyses, data were imported into Proteome Discoverer 2.4 (Thermo Fisher Scientific), where quantitative signals correlating the TMTPro reporter ions (m/z 126, 127N, 127C, etc.) were extracted. In addition to quantitative signal extraction, the MS/MS data were searched against the SwissProt *mus musculus* database (downloaded in November 2019), a common contaminant/spiked protein database (bovine albumin, bovine casein, yeast ADH, etc.), and an equal number of reversed-sequence "decoys" for false discovery rate determination. Mascot Distiller and Mascot Server (version 2.5, Matrix Sciences) were used to produce fragment ion spectra and to perform the database searches. Database search parameters included fixed modification on Cys (carbamidomethyl) and variable modification on Met (oxidation), Lys (TMT), and peptide N-termini (TMT). Precursor mass tolerances were 2.0 ppm and product ion mass tolerances were 0.02 Da with full trypsin enzyme rules required. Peptide Validator and Protein FDR Validator nodes in Proteome Discoverer were used to annotate the data at a maximum 1% protein false discovery rate based on q-value calculations. Peptide homology was addressed using razor rules in which a peptide matched to multiple different proteins was exclusively assigned to the protein that has more identified peptides. Protein homology was addressed by grouping proteins that had the same set of peptides to account for their identification. A master protein within a group was assigned based on % coverage.

Before imputation, a peptide filter was deployed which required a peptide to have a quantitative value in >50% of the samples within a group (i.e., wt or ko). After that filter, any missing data missing values were imputed using the following rules: (1) if only a single signal was missing within the group of three, an average of the other two values was used; or (2) if two of three signals were missing within the group of three, a randomized intensity within the bottom 2% of the detectable signals was used. To summarize to the protein level, all peptides belonging to the same protein were summed into a single intensity. The protein level data were then intensity normalized using a robust mean normalization in which the highest and lowest 10% of the signals were excluded, and then the average of the remaining signals was made to be the same across each individual channel. The normalized, protein level data were used for the remainder of the analysis. The protein network was visualized in Cytoscape (version 3.7.2). Known protein interactions were mapped using STRING and BioGRID databases. Functional annotation and enrichment were done by using a combination of DAVID and GeneCards resources. TMT data and functional annotations can be found in Extended Data Table 10-1. All proteomics data will be made publicly available on ProteomeExchange database.

Statistical analysis. Details about experimental replicates and the statistical tests used are given in the figure legends. All experiments were replicated at least 3 times. Statistical analysis and plotting were performed with GraphPad Prism (GraphPad Software) or Microsoft Excel. Data were tested for normal distribution using the Shapiro-Wilk test to determine the use of parametric or nonparametric tests. Appropriate *post hoc* tests were conducted in analyses with multiple comparisons and are also stated in the figure legends. Two tailed p values are reported for t tests. For all graphs, values are expressed as mean ± SEM.

Data availability. Raw proteomics data will be made available in the Proteome Exchange database. The rest of the datasets generated during and/or analyzed in the current study are available from the corresponding author on reasonable request.

Results

Generation of *Cnksr2*$^{-/Y}$ mice

Model organisms to study EAS are critically needed to understand this devastating disorder's underlying pathogenesis. Despite strong human genetic evidence implicating *CNKSR2* loss-of-function mutations, there have been no *in vivo* studies of Cnksr2 loss of function. Conditional *Cnksr2*$^{-/Y}$ KO mice, flanking exon 2 of *Cnksr2* with *loxP* sites, were generated to determine whether this new mouse could phenotypically model EAS. Following germline transmission with a constitutive *Flp*-deleter line to remove the neomycin selection cassette, floxed mice were crossed with CMV promoter-driven Cre-recombinase mice to create a *Cnksr2* KO line (Fig. 1*A*,*B*). Targeted mass spectrometry of purified synaptosomes confirmed the lack of Cnksr2 protein in *Cnksr2*$^{-/Y}$ mice by quantifying three different peptides (Fig. 1*D*,*G*). Hemizygous KO males (*Cnksr2*$^{-/Y}$) and littermate controls (*Cnksr2*$^{+/Y}$) were used in all experiments. *Cnksr2*$^{-/Y}$ mice were grossly normal in appearance with no significant difference in body weight between adult WT and KO mice (Fig. 1*C*). Additionally, histochemistry analysis revealed no significant differences in neuronal cell densities in *Cnksr2*$^{+/Y}$ and *Cnksr2*$^{-/Y}$ brains in the cortex and hippocampus demonstrating no gross changes in the morphology (Fig. 1*H*).

Cnksr2 is expressed in cortical, subcortical, and cerebellar regions during postnatal development

To better understand Cnksr2 neuronal expression patterns, given that EAS is a neurodevelopmental disorder, *Cnksr2* mRNA levels throughout postnatal development (P0, P12, and P60) were investigated using ISH of sagittal brain sections. Controls included probes for *dapB* (bacterial gene; negative control) and *Ppib* (housekeeping gene; positive control) (Fig. 2*A*). Prominent expression of *Cnksr2*, as early as postnatal day 0 (P0), was observed in the cortex, hippocampus, striatum, and cerebellum, with little to no expression observed midbrain, thalamus, and hypothalamus (Fig. 2*B*). This expression pattern is surprisingly similar to the expression pattern reported for *Grin2a* (Lein et al.,

Table 1. Summary of clinical reports on CNKSR2 patients

	Houge et al., 2012	Vaags et al., 2014	Vaags et al., 2014	Aypar et al., 2015	Damiano et al., 2017	Sun et al., 2018	Bonardi et al., 2020	Daoqi et al., 2020
Number of patients	1	5	3	1	2	1	4	1
Age(s)	5	8/12/13/6/8	56/58/62	7	12/18	8	5/21/12/9	5.5
CNKSR2 variant(s)	Deletion at Xp22.12	Deletion at Xp22.12	Frameshift mutation p.D152RfsX8	Deletion at Xp22.12	Nonsense mutation p.Arg712*	Nonsense mutation p.Arg729*	p.Glu675Glyfs*41 p.T83Kfs*30 p.Tyr153Serfs*5 Deletion at Xp22.12	Deletion of exon 14-17
Intellectual disability	Mild to moderate 1/1	5/5	3/3	1/1	3/3	1/1	Mild/moderate 2/4	1/1
Epilepsy/seizures	1/1	4/5	3/3	1/1	2/2	1/1	4/4	1/1
CSWS	NR	5/5	NR	NR	2/2	1/1	4/4	1/1
ADHD	1/1	5/5	3/3	NR	2/2	1/1	2/4	1/1
Language delay/loss	1/1	5/5	3/3	0/1	2/2	1/1	4/4	1/1

Clinical studies identifying CNKSR2 variants in patients. NR, Not reported.

2007). Given the high expression of *Cnksr2* in cortical areas and the cognitive deficits seen in EAS patients, subsequent analyses of how the loss of Cnkrs2 may alter neuronal function were focused on these regions.

Cnksr2 loss leads to increased spontaneous firing and bursting rates of cortical neurons *in vitro*

To investigate whether the loss of Cnksr2 influences neuronal firing, MEA recordings were used. MEA enables the high throughput, simultaneous local extracellular field recordings of neuronal samples over time *in vitro*, revealing potential disturbances to neuronal network activity in the same cells during neural development (Chiappalone et al., 2006; Lu et al., 2016). Dissociated cortical neurons from *Cnksr2*$^{-/Y}$ and WT control littermate mice were plated and their spontaneous activity was recorded every 2 d from DIV6 to DIV12 (Fig. 3*A*). Individual spikes were identified by threshold-based spike detection and used for raster plots and subsequent data analysis (Fig. 3*B–D*). Both *Cnksr2*$^{-/Y}$ and WT neurons displayed synchronized firing from DIV6 onwards. Remarkably, *Cnksr2*$^{-/Y}$ neurons displayed significantly increased mean firing rates at every time point from DIV6 to DIV12 (~21%-38% increase; Fig. 3*C*). In addition, there was also a significant increase in burst frequency in *Cnksr2*$^{-/Y}$ neurons compared with the WT controls at each time point (~17%-50% increase; Fig. 3*D*). These results show that the loss of Cnksr2 significantly alters neuronal physiology during development *in vitro*, resulting in the increased firing of cortical neurons. Next, to further explore this hyperactivity phenotype, the neural activity measurements were performed *in vivo*.

Cnksr2$^{-/Y}$ mice exhibit abnormal EEGs with epileptiform discharges

Many children with EAS develop recurrent seizures (epilepsy) and display abnormal EEG patterns. To quantify the effect of Cnksr2 loss on EEG phenotypes, video EEG and EMG were simultaneously recorded in *Cnksr2*$^{-/Y}$ and WT mice of 6-8 weeks of age (Fig. 4*A*). Two EEG electrodes were implanted on the dura (occipital: EEG1; central: EEG2), and the EMG wires were placed under the neck muscle. Comparison of the total EMG signal power revealed no differences between genotypes (Fig. 4*B*). Next, an automated line length search method (ALLSM) (Bergstrom et al., 2013) was used to identify electrographic seizure events lasting at least 10 s in both WT and KO EEG recordings. Events detected by the algorithm were further analyzed by manual inspection of the EEGs and synchronized video recordings. The patterns were consistent with electrographic seizure as evident in the abrupt onset of spike and polyspike wave activity (Fig. 4*E*,*G*,*H*), and the activity was typically present in either the central (EEG2) or the occipital (EEG1) electrode. These were identified in each of the KO animals with the number ranging from 1 to 13 per day. A single event was detected by the algorithm in a single WT animal; manual review together with correlation of video led to the conclusion that activity detected on EEG was caused by animal movement and was not of cerebral origin. Notably, no overt behavioral change was associated with these electrographic seizures.

In addition to these electrographic seizures, brief spike-wave events (duration 1-2 s) (Fig. 4*D*) were detected by the algorithm in *Cnksr2*$^{-/Y}$ animals (40 events/h on average), and almost no events were detected in Cnksr2$^{+/Y}$ animals. It has been documented that WT mice can exhibit epileptiform spikes at low rates (Purtell et al., 2018).

Furthermore, rare behavioral seizures consisting of tonic and/or clonic activity of all four limbs lasting 30-60 s were observed in *Cnksr2*$^{-/Y}$ mice during routine handling of mice. A total of three events were detected in 3 Cnksr2$^{-/Y}$ mice (see example Movie 1). None of these events was detected in WT mice.

Next, vigilance states in which seizure events occur were identified using δ frequency spectral power analysis (Rachalski et al., 2014; Soltani et al., 2019). Three states were identified as wake/REMS, NREMS, and transition state between wake/REMS to NREMS (Fig. 4*J*). Analysis showed that the majority of the events occurred during NREMS or during transition state ($n = 23$). These results demonstrate that loss of Cnksr2 leads to abnormal EEGs and increased susceptibility for spontaneous seizures. Whether the electrophysiological changes observed in the *Cnksr2*$^{-/Y}$ mice are associated with abnormal behaviors was next evaluated.

Cnksr2 KO mice display increased anxiety and impaired behavioral flexibility

Elevated neuronal excitation and seizures are often comorbid in neurologic disorders that present with behavioral abnormalities (Rubenstein and Merzenich, 2003; Rakhade and Jensen, 2009; Yizhar et al., 2011). Human patients with *CNKSR2* mutations exhibit seizures, cognitive deficits that can range from mild to severe, aphasia, and ADHD (Table 1). To evaluate the effect of Cnksr2 loss on mouse behavior, locomotive and exploratory behaviors were first assessed using the open field test (Fig. 5*A*). During the 1 h testing session, *Cnksr2*$^{-/Y}$ mice spent significantly less time in the center area of the arena compared with WT littermates and showed decreased vertical activity, which is indicative of increased anxiety. In contrast, no significant effect of genotype was observed in the total distance traveled in the arena. Elevated zero maze

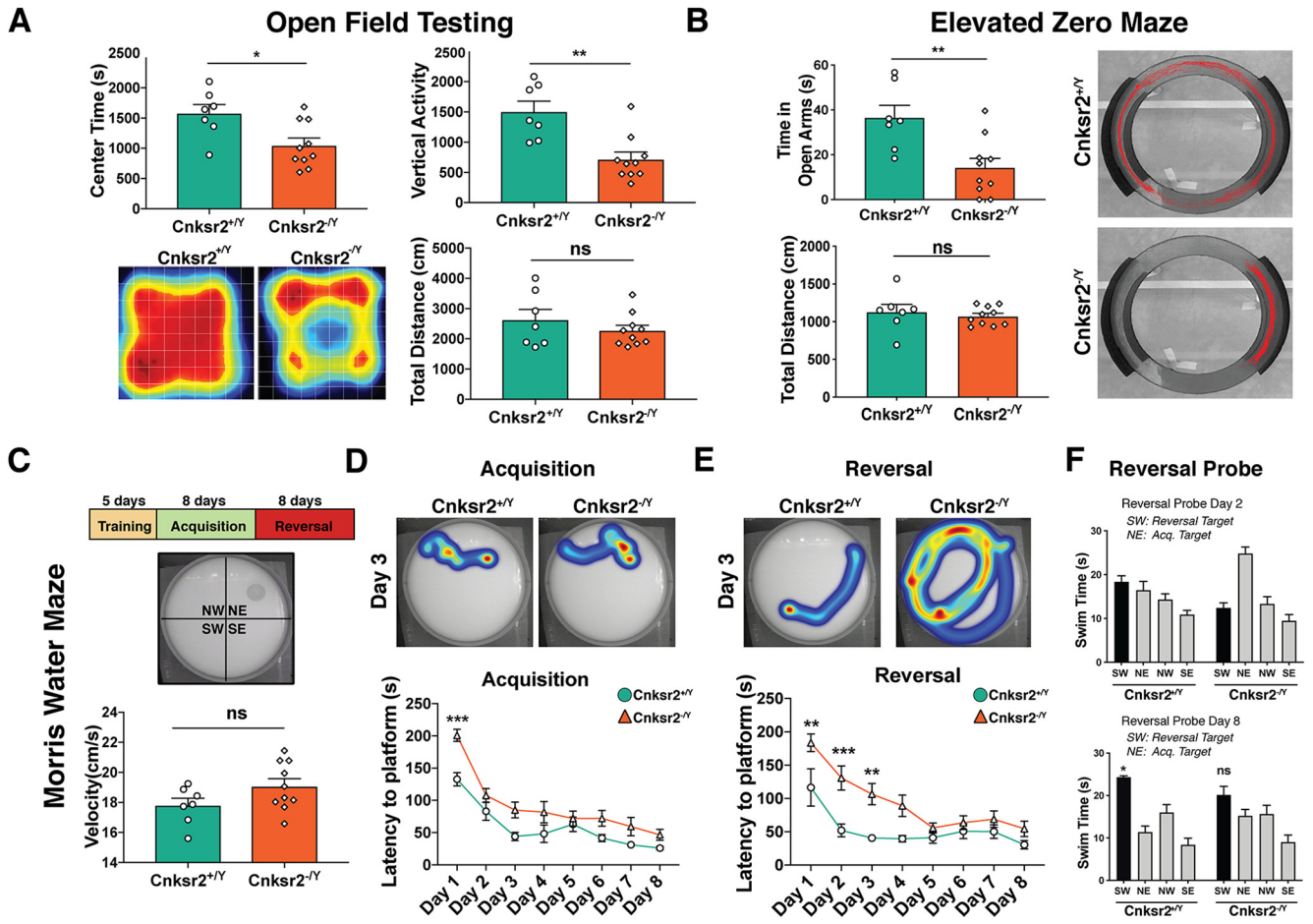

Figure 5. Loss of Cnksr2 causes increased anxiety and impaired reversal learning. ***A***, Open field testing data for time in center, vertical activity, and total distance moved. *Cnksr2*$^{-/Y}$ mice spent significantly less time (*$p = 0.013$; unpaired *t* test) in the center area but did not show any difference in total distance traveled ($p > 0.05$; unpaired *t* test). *Cnksr2*$^{-/Y}$ mice also had decreased vertical activity (**$p = 0.001$; unpaired *t* test). Representative heat map shows locomotion traces for both *Cnksr2*$^{+/Y}$ and *Cnksr2*$^{-/Y}$ during 1 h exploration session. ***B***, Elevated zero maze data. The percentage of time spent in the open areas of the elevated zero maze and the total distance traveled is shown for each genotype. *Cnksr2*$^{-/Y}$ mice spent significantly less time in the maze's open areas than *Cnksr2*$^{+/Y}$ mice (**$p = 0.004$; unpaired *t* test). *Cnks2*$^{+/Y}$ and *Cnksr2*$^{-/Y}$ mice did not show any differences in the total distance traveled ($p > 0.05$; unpaired *t* test). Data are mean ± SEM. Representative locomotion traces during testing session for each genotype are shown. ***C***, Morris Water Maze testing data. Top, Schematic for the experimental plan and a representative image of quadrants within the pool. Bottom, No difference in swim velocities was found between genotypes ($p > 0.05$; unpaired *t* test). Data are mean ± SEM. Mice were tested in two daily sessions of four trials each for both acquisition and reversal phases. ***D***, Acquisition phase of the water maze test. Top, Representative heat map traces of *Cnksr2*$^{+/Y}$ and *Cnksr2*$^{-/Y}$ mice during a single trial on day 3 of acquisition. Bottom, Graph of session averages ± SEM is represented. On the first day of the acquisition phase, *Cnksr2*$^{-/Y}$ mice spent significantly more time to reach the platform: ***$p = 0.0006$ (two-way ANOVA with Bonferroni's multiple comparisons). *Cnksr2*$^{-/Y}$ mice performed similarly to *Cnksr2*$^{+/Y}$ mice for days 2-8. ***E***, Reversal phase. Top, Representative single-trial heat map traces of *Cnksr2*$^{+/Y}$ and *Cnksr2*$^{-/Y}$ mice during a single trial on day 3 of reversal. Bottom, Graph of session averages ± SEM is represented. During reversal testing, *Cnksr2*$^{-/Y}$ mice spent significantly more time to reach the platform on the first 3 d of testing: **$p < 0.01$; ***$p < 0.001$ (two-way ANOVA with Bonferroni's multiple comparisons). ***F***, Reversal probe trials. Graphs of swim times for *Cnksr2*$^{+/Y}$ and *Cnksr2*$^{-/Y}$ within each quadrant on day 2 (top) and day 8 (bottom) are shown. On day 8, *Cnksr2*$^{+/Y}$ mice spent significantly more time in the target quadrant than the nontarget quadrants: $p < 0.05$ (two-way ANOVA with Sidak's multiple comparisons). For *Cnksr2*$^{-/Y}$, the difference was not significant.

testing was used to analyze anxiety-like behavior further (Fig. 5*B*). *Cnksr2*$^{-/Y}$ mice spent less time in the maze's open arms compared with WT littermate controls, whereas the total distance traveled was similar between groups. These results demonstrate that loss of Cnksr2 increases anxiety-like behavior in mice but does not affect general locomotion skills.

Morris water maze testing was next used to investigate spatial learning and memory in *Cnksr2*$^{-/Y}$ mice (Fig. 5*C–F*). On the first day of acquisition testing, *Cnksr2*$^{-/Y}$ mice took significantly more time to reach the hidden platform than WT controls but showed similar performance on days 2-8. During acquisition probe testing, both WT and *Cnksr2*$^{-/Y}$ mice showed an increased preference for the target versus the nontarget quadrants throughout the test (Fig. 5*D*). In the reversal-learning phase, *Cnksr2*$^{-/Y}$ mice took significantly more time to find the hidden platform on days 1-3 compared with WT littermates (Fig. 5*E*). Consistent with learning and memory deficits, *Cnksr2*$^{-/Y}$ mice also showed impairments in all probe tests during reversal, never distinguishing the new target from the nontarget quadrants (Fig. 5*F*). In contrast, WT littermates showed a clear preference for the target over nontarget quadrants by day 6. No significant difference in swim velocity between genotypes was found, eliminating the possibility that swim speed may have been a contributing factor. These results show that *Cnksr2*$^{-/Y}$ mice have impaired cognitive flexibility.

Additionally, the working memory and episodic memory of *Cnksr2*$^{-/Y}$ mice were assessed using Y-maze spontaneous alternation, novel object recognition, and memory load testing. WT and *Cnksr2*$^{-/Y}$ mice engaged in a similar number of alternations in the Y-maze, suggesting intact working memory function (Fig. 6*A*). For episodic-like memory testing, KO performance was

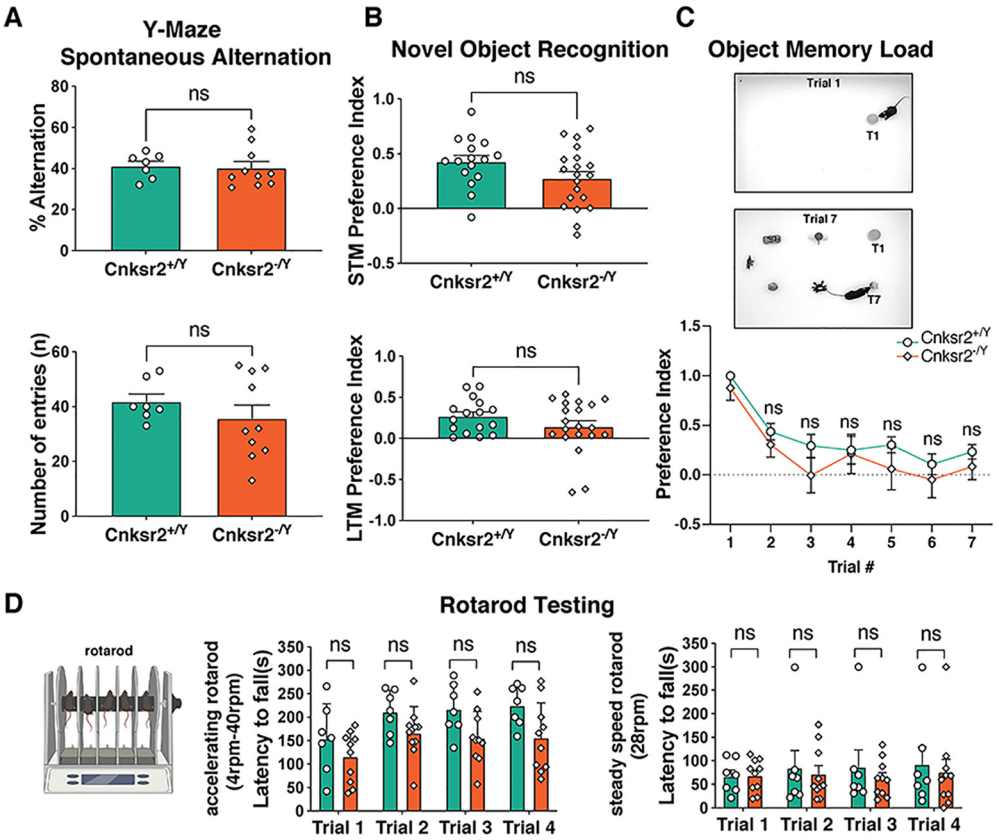

Figure 6. Behavioral characterization of Cnksr2 KO mice. ***A***, Y-Maze spontaneous alternation test to evaluate working memory. No significant difference in % alternation and number of entries between genotypes: $p > 0.05$ (unpaired *t* test). ***B***, Novel object recognition to evaluate episodic-like memory. No significant difference in short-term memory (STM) or long-term memory (LTM) preference index: $p > 0.05$ (unpaired *t* test). ***C***, Object memory load testing to evaluate complex episodic-like memory. Top, Views of the testing arena in Trials 1 and 7. Bottom, No significant difference between genotypes in preference index across Trials 2-7: $p > 0.05$ (unpaired *t* test). ***D***, Rotarod testing. No significant difference in latency to fall in accelerating rotarod and steady speed rotarod between genotypes: $p > 0.05$ (two-way ANOVA, multiple comparisons with Bonferroni correction).

indistinguishable between genotypes in the novel object recognition task and memory load (Fig. 6*B*,*C*). Also, the evaluation of motor coordination using the rotarod test found no significant differences between WT and *Cnksr2*$^{-/Y}$ mice in the latency to fall (Fig. 6*D*). The effects observed here on cognitive performance suggest that Cnksr2 KO mice have mild deficits, phenocopying some aspects of cognitive deficits seen in patients with EAS.

Cnksr2$^{-/Y}$ mice exhibit a progressive loss of USVs absent of social interaction abnormalities

One of the cardinal features of EAS caused by mutations in *CNKSR2* is a progressive loss of vocal language (Deonna, 1991; Tassinari et al., 2000). To address whether *Cnksr2*$^{-/Y}$ mice display any vocal communication deficits, USVs emitted by pups during maternal separation were recorded and analyzed. No significant genotype effect was observed in the percentage of vocal pups or the number of calls per minute (Fig. 7*C*). However, the characteristics of the calls of the KO pups were significantly different from controls. Compared with WT littermates, *Cnksr2*$^{-/Y}$ pups displayed a significant decrease in the average duration of ultrasonic calls and a significant increase in call pitch (Fig. 7*C*). To investigate how these abnormalities in pups translated to adult communication, USVs in male mice were recorded and analyzed during courtship-based social interactions with an estrus female mouse. For *Cnksr2*$^{-/Y}$ adults, the percentage of vocal animals, the number of calls per minute, and average call duration were significantly lower than that of WT littermates (Fig. 7*D*). The three-chamber sociability test was performed to determine whether the vocalization deficits in adult male mice resulted from an altered social drive. No significant effect of genotype for sociability was observed (Fig. 7*D*). Together, these results indicate that the deficits in adult USVs of the *Cnksr2*$^{-/Y}$ mice were not a result of altered motivation for social interactions. Our findings demonstrate that loss of Cnksr2 leads to a progressive loss of communicative vocalizations in mice (Fig. 7*B*), which is remarkably consistent with human *CNKSR2* patient aphasia. Given Cnksr2 KO mouse model recapitulates behavioral and electrophysiological disruptions seen in the patients, the molecular roles of Cnksr2 were investigated next to provide insights into the etiology of EAS.

Cnksr2 is localized at excitatory and inhibitory postsynaptic sites

To provide initial insights into the role of Cnksr2 in neurons, the subcellular localization of Cnksr2 was explored. Since commercial antibodies to Cnksr2 have limited usefulness (Zieger et al., 2020), an alternative CRISPR-based strategy to visualize endogenous Cnksr2 was used. Canonical Cnksr2a isoform was tagged with a highly antigenic spaghetti-monster V5 (smFP-V5) (Viswanathan et al., 2015) donor sequence using HiUGE (Gao et al., 2019). An AAV HiUGE donor vector harboring smFP-V5 and a gRNA vector targeting the genomic coding sequence near the C-terminus of Cnksr2 were combined and used to transduce primary cortical neurons from Cas9 transgenic mice at 5 DIV (Fig. 8*A*). While targeting near the C-terminus results in deletion of PDZ-binding motif, previous studies (Iida et al., 2002; Zieger

et al., 2020) show that membrane localization of Cnksr2 relies on pleckstrin homology domain, which remains intact after HiUGE targeting. Immunofluorescence analysis at DIV14 (Fig. 8*C*) revealed that smFP-V5 labeled Cnksr2 is localized at excitatory postsynaptic sites and colocalized with both Homer1 (Homer Postsynaptic Density Scaffold Protein 1) and Vglut1 (Vesicular Glutamate Transporter 1). Interestingly, the presence of Cnksr2 labeling at inhibitory postsynaptic sites was also sporadically observed (Fig. 8*D*) as evidenced by colocalization with Gephyrin and VGAT (Vesicular GABA Transporter). Further quantification revealed that ~45% of the Cnksr2 puncta colocalized with Homer1 and ~13% of the Cnksr2 puncta colocalized with Gephyrin (Fig. 8*E*). These observations are in line with the recent report of Cnksr2's synaptic localization using PSD-95 and Synapsin as markers (Lim et al., 2014; Zieger et al., 2020) and the proteomic identification of Cnksr2 at inhibitory postsynapses in our previous study (Uezu et al., 2016). Further, the labeling fidelity was confirmed by genomic PCR detection of smFP-V5 integration at the Cnksr2 locus and Western blot detection of the Cnksr2-smFP-V5 fusion protein at the expected molecular mass (~160 kDa) (Fig. 8*B*).

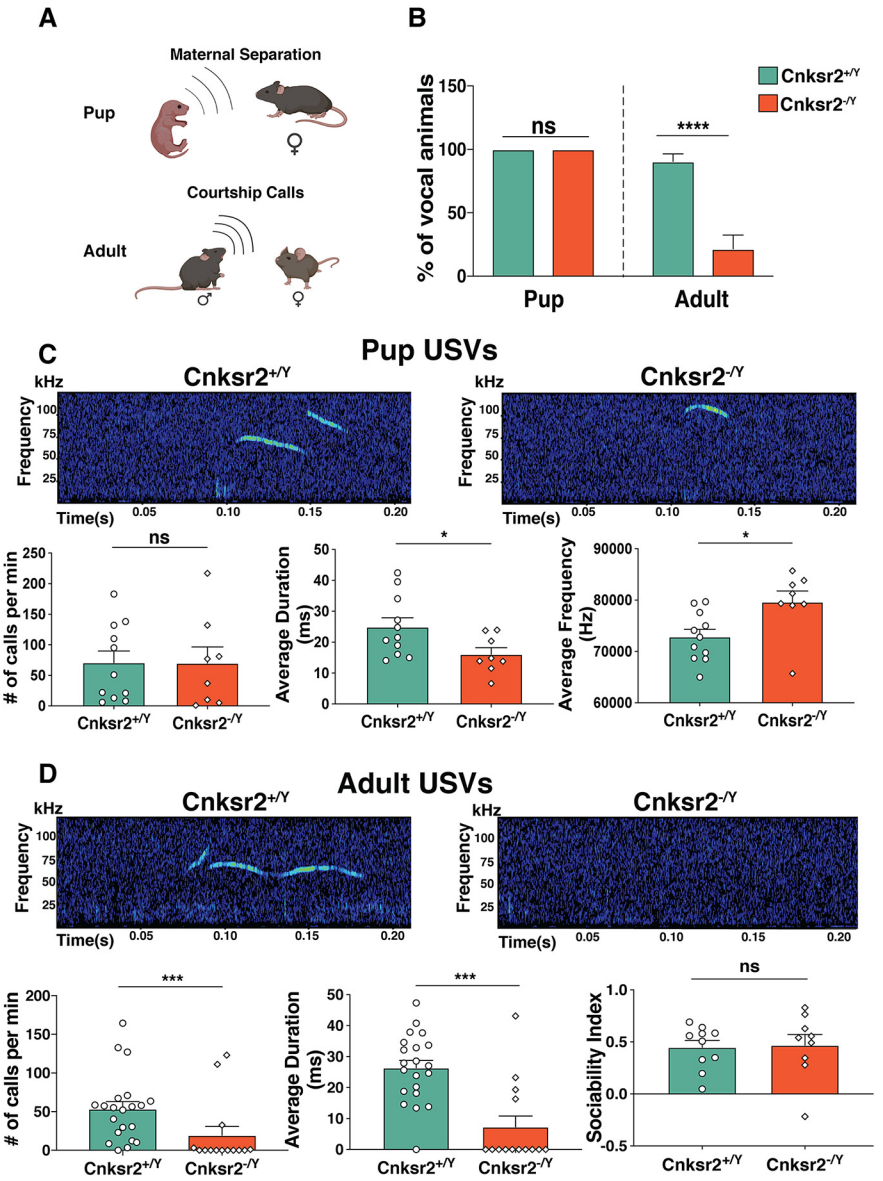

Figure 7. *Cnksr2*$^{-/Y}$ mice show USV deficits but not impairment of social interaction behavior. ***A***, Schematic of experimental design. Pup vocalizations were recorded during maternal separation on P5. Adult male vocalizations were recorded during courtship behavior. ***B***, Graphs of percent of vocal animals per genotype for pup and adult assays. No significant difference was observed in the percent of vocal pups between genotypes. In contrast, a significant decrease in percent vocal adults was observed in Cnksr2$^{-/Y}$ mice compared with WT controls: ****$p < 0.0001$ (unpaired *t* test). ***C***, Top, Example pup spectrogram patterns of USVs. Bottom, Graphs of calls per min as well as average duration and frequency for each genotype. No significant difference was observed between genotypes in the number of calls per min ($p > 0.05$, unpaired *t* test). Cnksr2$^{-/Y}$ pups showed decreased average call duration (*$p = 0.038$; unpaired *t* test) and increased call frequency (*$p = 0.016$; unpaired *t* test). ***D***, Top, Example spectrogram pattern of USVs in adult male mice during courtship. Bottom, Graphs of calls per min, average call duration, and social preference in the three-chamber sociability test for each genotype. Both numbers of calls per min (***$p = 0.0006$; Mann–Whitney test) and average call duration (***$p = 0.0002$; Mann–Whitney test) were significantly decreased in *Cnksr2*$^{-/Y}$ mice; however, there was no significant difference in sociability index demonstrated by three-chamber sociability test between *Cnksr2*$^{+/Y}$ and *Cnksr2*$^{-/Y}$ mice ($p > 0.05$; unpaired *t* test). Data are mean ± SEM.

The loss of Cnksr2 results in changes to the synaptic proteome

Cnksr2 has multiple protein interaction domains, and previous studies have identified many interactors of Cnksr2 with diverse functions consistent with its proposed role as a scaffolding protein (Fig. 9*A*,*B*). Together, these studies suggested that the loss of Cnksr2 might alter the proteins it spatiotemporally organizes, and this could contribute to the behavioral and functional phenotypes observed in Cnksr2 KO mice. To test whether the depletion of Cnksr2 alters the synaptic proteome, a mass spectrometry-based proteomics approach using TMT labeling for unbiased discovery and relative quantification of proteins was used (Fig. 9*C*). Since Cnksr2 is localized to the synapses and the previous *in vitro* studies of Cnksr2 have demonstrated its scaffolding role in hippocampal neurons (Lim et al., 2014; Zieger et al., 2020), synaptosomes were biochemically purified from *Cnksr2*$^{-/Y}$ and WT adult mice hippocampi and were used for this analysis. The TMT experiment identified 32,077 unique peptides corresponding to 3069 proteins. Quantitative comparison of *Cnksr2*$^{-/Y}$ and WT groups revealed 109 proteins whose levels were significantly altered (45 upregulated and 64 downregulated) in KO mice (Fig. 10*A*). Protein–protein interactions between differentially expressed proteins (DEPs) were significantly enriched ($p = 0.009$) compared with the expected number of edges from a random set of an equal number of proteins, suggesting a biologically connected network.

Among these proteins, Shank3, Cyth2, Cyth3, Arhgap39, Araf, and Ywhae were previously shown to interact with Cnksr2 (Fig. 10*B*). Gene ontology analyses showed enrichment in terms, such as small GTPase signaling ($n = 10$), ion transmembrane transport ($n = 13$), and synaptic vesicle membrane ($n = 11$). Other hits included cytoskeletal, mitochondrial, and metabolic

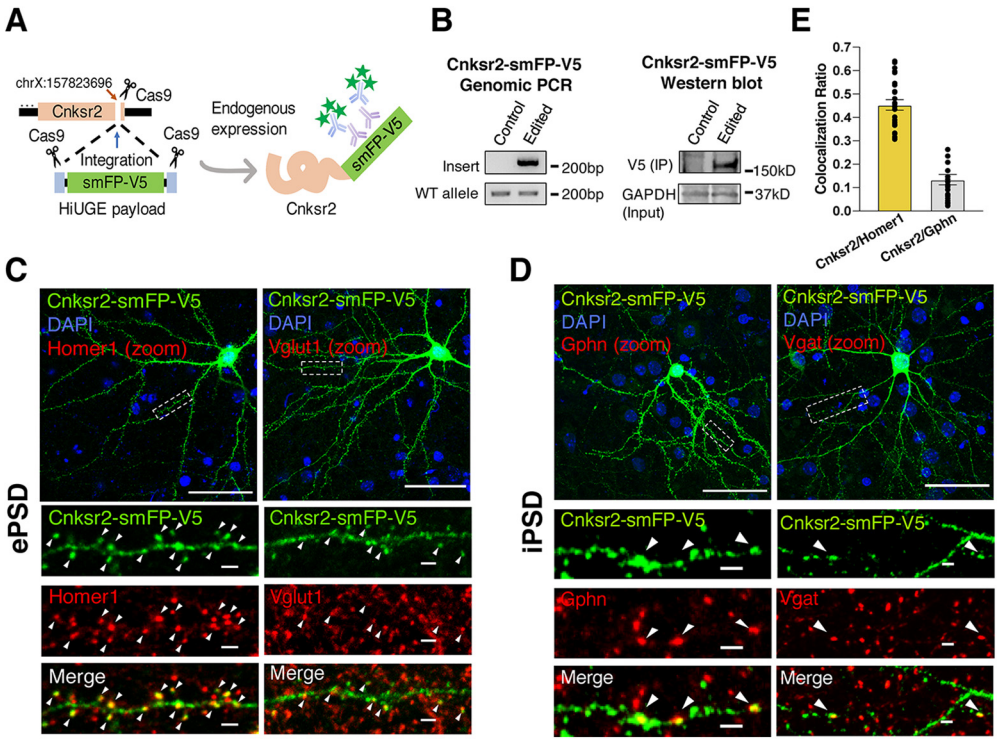

Figure 8. Cnksr2 is localized to the postsynapse. ***A***, Schematic for HiUGE labeling of endogenous Cnksr2. ***B***, Left, Genomic PCR detection of smFP-V5 integration at the Cnksr2 locus. Right, Western blot detection of the Cnksr2-smFP-V5 fusion protein at the expected molecular mass (~160 kDa). IP, Immunoprecipitation enrichment with V5-trap beads. ***C***, Top, Knock-in expression of Cnksr2-smFP-V5 in cultured neurons (green) and DAPI (blue) is shown. Scale bars, 40 μm. Bottom left, Higher-magnification view of the boxed region shows colocalization (arrowheads) of Cnksr2-smFP-V5 immunoreactivity with Homer1 immunosignal (red). Scale bar, 2 μm. Bottom right, Higher-magnification view of the boxed region shows colocalization (arrowheads) of Cnksr2-smFP-V5 immunoreactivity with Vglut1 immunosignal (red). Scale bar, 2 μm. ***D***, Top, Knock-in expression of Cnksr2-smFP-V5 in cultured neurons (green) and DAPI (blue). Scale bars, 40 μm. Bottom left, Higher-magnification view of the boxed region shows colocalization (arrowheads) of Cnksr2-smFP-V5 immunoreactivity with Gephyrin immunosignal (red). Scale bar, 2 μm. Bottom right, Higher-magnification view of the boxed region shows colocalization (arrowheads) of Cnksr2-smFP-V5 immunoreactivity with VGAT immunosignal (red). Scale bar, 2 μm. ***E***, Graph represents colocalization ratios for Cnksr2 puncta with Homer1 (mean value 0.45) and Gephyrin (mean value 0.13). Colocalization ratios were calculated as the number of Cnksr2 puncta colocalized with Homer1 or Gephryin divided by total number of Cnksr2 puncta. Two or three dendrites were imaged from eight or nine neurons from multiple coverslips.

proteins. Strikingly, 32 of the dysregulated proteins were previously implicated in neurologic disorders. Mapping specific patient phenotypes to these genes revealed that 26 were implicated with seizures, intellectual disability, and language abnormalities (Fig. 10*C*). These results give a comprehensive view of synaptic alterations in Cnksr2 KO mice that may underlie the behavioral and electrophysiological phenotypes.

Discussion

EAS remains an enigmatic disorder whose genetic and molecular basis is poorly understood. In this study, we report the analysis of a new mouse model based on *CNKSR2*, a strong X-linked candidate for EAS, and find that the mouse phenotypes strongly correlate to human reports.

To our knowledge, the *Cnksr2*$^{-/Y}$ mouse line is the first model of progressive aphasia-like phenotypes within an epilepsy disorder context. Previous studies have demonstrated that mutations in *CNKSR2* associated with neurodevelopmental disorders contain large deletions and nonsense mutations likely to be loss of function. Targeted mass spectrometry demonstrated that our mutation of mouse Cnksr2 resulted in a loss of protein expression, providing a model with strong construct validity for the proposed mechanism in human patients. Using behavioral testing and EEG analysis, we demonstrated that loss of Cnksr2 in mice produces similar behavioral and electrophysiological abnormalities observed in EAS. We thus establish the face validity of this new model and confirm *CNKSR2* loss of function as a novel driver of this disorder. Having established our model's construct and face validity, we further analyzed Cnksr2 expression, localization, and role in organizing the synaptic proteome.

We show that *Cnksr2* is expressed in the brain throughout postnatal development in the cortex, hippocampus, striatum, and cerebellum. We find that the endogenous Cnksr2 is localized at the excitatory and inhibitory postsynapses of cortical neurons, consistent with previously published studies (Lim et al., 2014; Uezu et al., 2016; Zieger et al., 2020). We show that the loss of Cnksr2 results in increased neuronal network activity using MEA and EEG recordings. Since Cnksr2 is expressed in both excitatory and inhibitory cells and in both excitatory and inhibitory synapses, its role in maintaining proper neuronal firing/activity is likely complex; thus, future studies using patch-clamp recordings along with cell-specific deletions of Cnksr2 are needed to tease out its cell-dependent synaptic functions.

One proposed function of Cnksr2 is that it acts as a synaptic scaffolding protein, essential for organizing and anchoring proteins important for synaptic physiology. By using a quantitative discovery mass spectrometry approach, we identified 109 proteins differentially expressed in the hippocampus of *Cnksr2*$^{-/Y}$ mice. These proteomic data highlight the diverse cellular processes downstream of Cnksr2 depletion. Below we discuss some of these dysregulated proteins and their pathways.

Six DEPs were previously known as Cnksr2 interactors (Shank3, Cyth2, Cyth3, Arhgap39, Araf, and Ywhae). Among these previously identified proteins, Arhgap39, a Rac1 GAP that

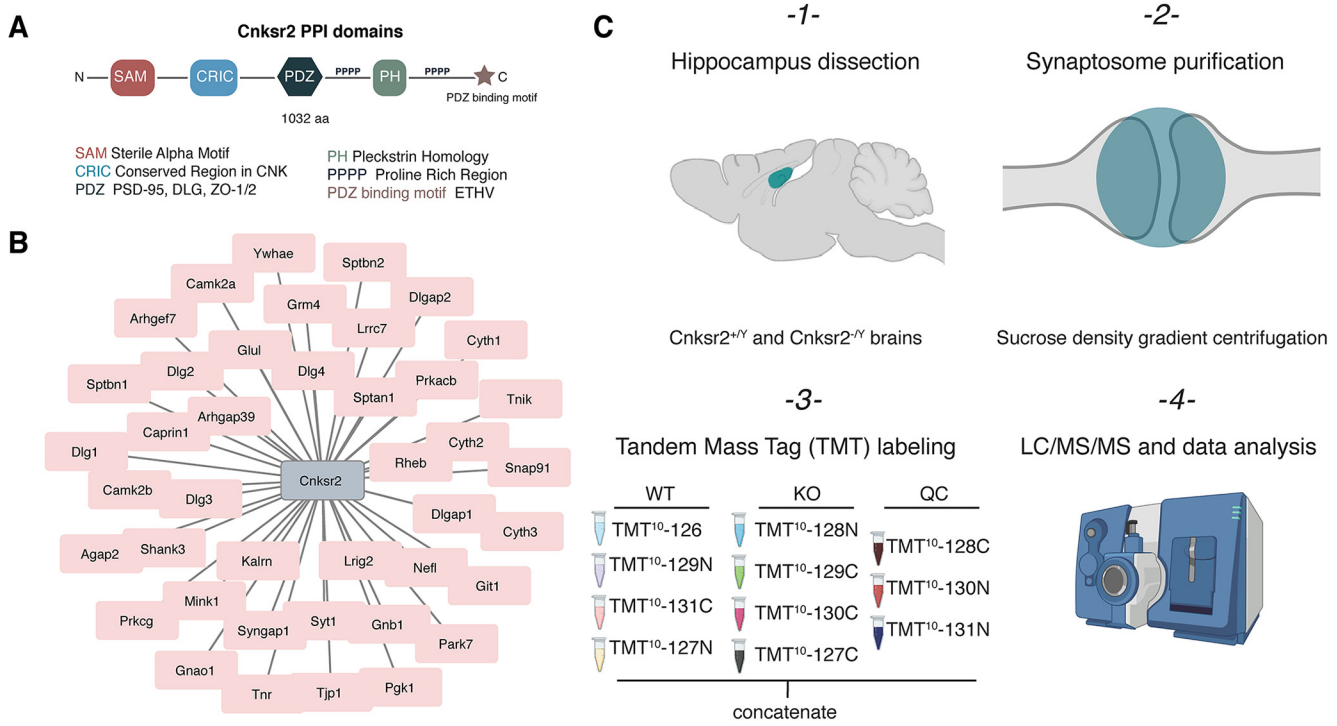

Figure 9. Cnksr2 as a scaffold protein and TMT proteomics workflow. ***A***, Domain structure of Cnksr2. ***B***, Cnksr2 interactor proteins. Curated from BioGRID and STRING databases. ***C***, Workflow for differential protein expression analysis using TMT11plex multiplexed tagging with fractionated LC-MS/MS. Figure created with www.BioRender.com.

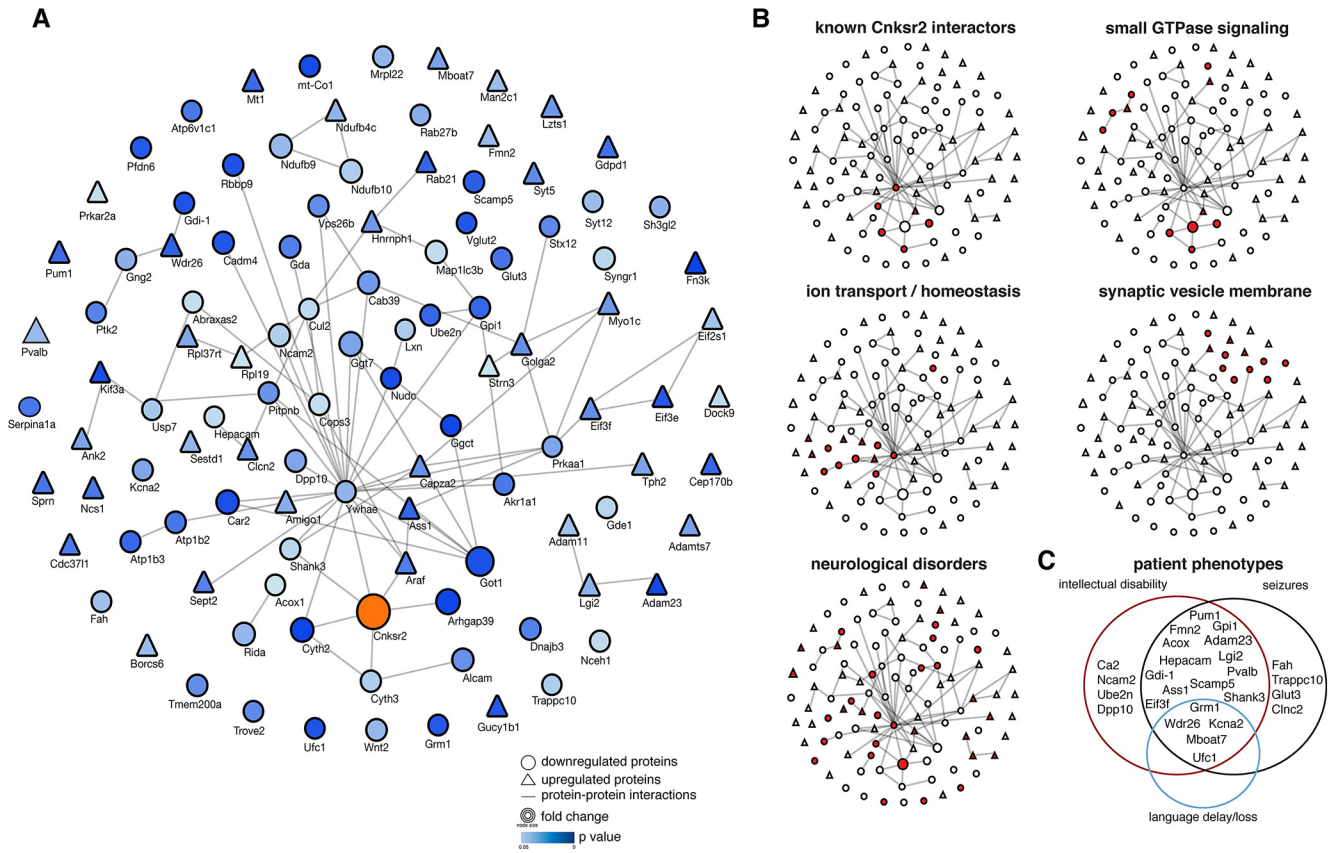

Figure 10. The loss of Cnksr2 results in changes to the synaptic proteome. ***A***, Network of dysregulated proteins in *Cnksr2*$^{-/Y}$ mice; 109 proteins were differentially expressed in synaptosomes between *Cnksr2*$^{-/Y}$ and *Cnksr2*$^{+/Y}$ mice (two-tailed heteroscedastic *t* test on log2-transformed data $p < 0.05$, $n = 4$ for *Cnksr2*$^{+/Y}$, *n* total = 4 for *Cnksr2*$^{-/Y}$ mice). See (Extended Data Table 1-1). ***B***, Clustergram topology of proteins (red) in selected functional categories. ***C***, Dysregulated proteins implicated in patient phenotypes of seizures, intellectual disability, and language delay/loss.

limits Rac1 activity, was the most affected (~65% depletion) in our synaptosome-derived dataset. This is in line with a previous study in which Arhgap39 was suggested to be the major binding partner of Cnksr2 (Lim et al., 2014). It is possible that the resulting synaptic depletion of Arhgap39 accounts for some of the phenotypes we report in Cnksr2 mice since Arhgap39 plays a role in synaptic plasticity and learning in mice (Lee et al., 2017; Nowak, 2018). In addition to Arhgap39, we identified other small GTPase signaling proteins ($n = 9$) that were differentially expressed, suggesting that this is a pathway altered by loss of Cnksr2.

Interestingly, several synaptic vesicle membrane proteins were also altered ($n = 11$). However, our proteomics and HiUGE labeling demonstrate that Cnksr2 is localized at postsynapses, and recent proteomics data do not suggest that Cnksr2 is localized to presynapses (Dube et al., 2020). Thus, it is possible that any changes to the presynapse are a result of altered neural activity or compensatory/homeostatic changes that arise from the loss of postsynaptic Cnksr2.

Ion transmembrane transport and homeostasis-related proteins were the most significantly enriched in our dataset ($n = 13$). Kcna2 belongs to the potassium voltage-gated channel family of proteins; and interestingly, Amigo1, Ywhae, and Dpp10 can function to regulate potassium channel regulator activity (Kagan et al., 2002; Zagha et al., 2005; Peltola et al., 2016). Potassium channels have pivotal roles in regulating neuronal excitability, and loss-of-function and gain-of-function variants in K^+ channels both lead to a variety of epilepsy-related disorders (Brenner and Wilcox, 2012; Syrbe et al., 2015; Niday and Tzingounis, 2018).

Another epilepsy-related protein complex in our dataset was Adam11-Lgi2-Adam23. Mutations in LGI1 (a close relative of LGI2) that impair binding to Adam23 cause autosomal-dominant partial epilepsy with auditory features (ADPEAF) in humans (Kalachikov et al., 2002). Lgi1/Adam ligand/receptor complexes also modulate AMPAR-mediated synaptic transmission (Fukata et al., 2006) and contribute to neuronal morphology patterning (Owuor et al., 2009). While the molecular function of Lgi2 is not as well understood, *Lgi2* mutations cause focal epilepsy in dogs (Seppala et al., 2011). Moreover, a recent study suggests that Lgi2 plays a role in inhibitory synapse formation (Favuzzi et al., 2019). More work is needed to understand whether these DEPs individually or in combination may underlie the increased network activity and seizure phenotypes reported in our study. The DEPs we detected hint at complex signaling networks controlled by the putative scaffolding activity of Cnksr2 and provide a better understanding of specific downstream disruptions that CNKSR2 mutations may cause.

One of the core symptoms of EAS is epileptiform activity during sleep. Notably, the majority of the epileptiform activity detected in *Cnksr2*$^{-/Y}$ mice occurred during NREMS or during transition to NREMS, suggesting that *Cnksr2*$^{-/Y}$ may capture this feature of the disorder. It is possible that epileptiform activity influences cognitive abilities since it is often comorbid with intellectual disability, including in patients with *CNKSR2* mutations (Houge et al., 2012; Vaags et al., 2014; Aypar et al., 2015; Hu et al., 2016; Damiano et al., 2017; Sun et al., 2018; Polla et al., 2019; Bonardi et al., 2020; Daoqi et al., 2020). Indeed, *Cnksr2*$^{-/Y}$ mice exhibit cognitive inflexibility and anxiety consistent with intellectual disability symptoms observed in patients with intellectual disability. Using conditional mutagenesis in specific brain regions and cell types, it may be possible in future studies to investigate whether seizures are causative for the cognitive deficits observed.

Acquired aphasia is one of the most severe deficits seen in EAS disorders. Many patients have language difficulties, which coincide with the occurrence and worsening of seizures (Bonardi et al., 2020). Given that loss of speech and/or language can have devastating impacts on the patients, understanding the mechanisms underlying aphasia is critical. In mice, vocal expressions, such as USVs, are not learned but rather are innate expressions similar to humans' innate expressions (Mahrt et al., 2013). Despite this limitation, cortico-striatal circuits similar to those that control learned vocalizations in humans are also involved in USV production in mice (Arriaga et al., 2012). Additionally, projections from the ACC to periaqueductal gray are important for USVs, and the ACC in humans is involved in the control of emotional vocal utterances and other paralinguistic features of speech (Arriaga and Jarvis, 2013; Nieder and Mooney, 2020). Mouse USVs are extensively used in studies to model human vocal communication and associated disorders (Fischer and Hammerschmidt, 2011; Chabout et al., 2016; Wang et al., 2016). Indeed, our data show that *Cnksr2*$^{-/Y}$ mice display a progressive loss of USVs. Cnksr2 KO pups have increased pitch and decreased duration of ultrasonic calls. Remarkably, KO of another EAS-associated gene, *Grin2a*, also results in a similar USV phenotype in pups, with the pitch of the calls being consistently higher than controls around P5 (Salmi et al., 2019). This suggests the intriguing possibility that increased pitch may be an early marker of vocalization deficits common to EAS mouse models. *Cnksr2*$^{-/Y}$ adult mice also lose their ability to vocalize almost entirely, paralleling the language deficits observed in human CNKSR2 patients. Future work will be needed to understand the neural circuitry affected by Cnksr2 loss in the context of vocalizations.

In conclusion, our study supports that Cnksr2 loss in humans is a strong driver of EAS and reveals molecular perturbations and complex alterations in neuronal excitation associated with its related phenotypes in mice. This model provides a genetic and molecular framework for future studies of the disease etiology and the relationships between seizures, cognitive disability, and communication deficits.

References

Arriaga G, Jarvis ED (2013) Mouse vocal communication system: are ultrasounds learned or innate? Brain Lang 124:96–116.

Arriaga G, Zhou EP, Jarvis ED (2012) Of mice, birds, and men: the mouse ultrasonic song system has some features similar to humans and song-learning birds. PLoS One 7:e46610.

Aypar U, Wirrell EC, Hoppman NL (2015) CNKSR2 deletions: a novel cause of X-linked intellectual disability and seizures. Am J Med Genet A 167:1668–1670.

Bergstrom RA, Choi JH, Manduca A, Shin HS, Worrell GA, Howe CL (2013) Automated identification of multiple seizure-related and interictal epileptiform event types in the EEG of mice. Sci Rep 3:1483.

Bonardi CM, Mignot C, Serratosa JM, Giraldez BG, Moretti R, Rudolf G, Reale C, Gellert PM, Johannesen KM, Lesca G, Tassinari CA, Gardella E, Moller RS, Rubboli G (2020) Expanding the clinical and EEG spectrum of CNKSR2-related encephalopathy with status epilepticus during slow sleep (ESES). Clin Neurophysiol 131:1030–1039.

Brenner R, Wilcox KS (2012) Potassium channelopathies of epilepsy. In: Jasper's basic mechanisms of the epilepsies (Noebels JL, Avoli M, Rogawski MA, Olsen RW, Delgado-Escueta AV, eds). Bethesda, MD: National Center for Biotechnology Information.

Bumeister R, Rosse C, Anselmo A, Camonis J, White MA (2004) CNK2 couples NGF signal propagation to multiple regulatory cascades driving cell differentiation. Curr Biol 14:439–445.

Carvill GL, Regan BM, Yendle SC, O'Roak BJ, Lozovaya N, Bruneau N, Burnashev N, Khan A, Cook J, Geraghty E, Sadleir LG, Turner SJ, Tsai

MH, Webster R, Ouvrier R, Damiano JA, Berkovic SF, Shendure J, Hildebrand MS, Szepetowski P, et al. (2013) GRIN2A mutations cause epilepsy-aphasia spectrum disorders. Nat Genet 45:1073–1076.

Chabout J, Sarkar A, Patel SR, Radden T, Dunson DB, Fisher SE, Jarvis ED (2016) A Foxp2 mutation implicated in human speech deficits alters sequencing of ultrasonic vocalizations in adult male mice. Front Behav Neurosci 10:197.

Chiappalone M, Bove M, Vato A, Tedesco M, Martinoia S (2006) Dissociated cortical networks show spontaneously correlated activity patterns during in vitro development. Brain Res 1093:41–53.

Chiou SH, Winters IP, Wang J, Naranjo S, Dudgeon C, Tamburini FB, Brady JJ, Yang D, Gruner BM, Chuang CH, Caswell DR, Zeng H, Chu P, Kim GE, Carpizo DR, Kim SK, Winslow MM (2015) Pancreatic cancer modeling using retrograde viral vector delivery and in vivo CRISPR/Cas9-mediated somatic genome editing. Genes Dev 29:1576–1585.

Damiano JA, Burgess R, Kivity S, Lerman-Sagie T, Afawi Z, Scheffer IE, Berkovic SF, Hildebrand MS (2017) Frequency of CNKSR2 mutation in the X-linked epilepsy-aphasia spectrum. Epilepsia 58:e40–e43.

Daoqi M, Guohong C, Yuan W, Zhixiao Y, Kaili X, Shiyue M (2020) Exons deletion of CNKSR2 gene identified in X-linked syndromic intellectual disability. BMC Med Genet 21:69.

Deonna TW (1991) Acquired epileptiform aphasia in children (Landau-Kleffner syndrome). J Clin Neurophysiol 8:288–298.

Dube S, Rácz B, Brown WE, Gao Y, Soderblom EJ, Yasuda R, Soderling SH (2020) Action potential-coupled Rho GTPase signaling drives presynaptic plasticity. bioRxiv 2020.2010.2007.330126.

Favuzzi E, Deogracias R, Marques-Smith A, Maeso P, Jezequel J, Exposito-Alonso D, Balia M, Kroon T, Hinojosa AJ, Maraver EF, Rico B (2019) Distinct molecular programs regulate synapse specificity in cortical inhibitory circuits. Science 363:413–417.

Fischer J, Hammerschmidt K (2011) Ultrasonic vocalizations in mouse models for speech and socio-cognitive disorders: insights into the evolution of vocal communication. Genes Brain Behav 10:17–27.

Fritz RD, Radziwill G (2011) CNK1 and other scaffolds for Akt/FoxO signaling. Biochim Biophys Acta 1813:1971–1977.

Fukata Y, Adesnik H, Iwanaga T, Bredt DS, Nicoll RA, Fukata M (2006) Epilepsy-related ligand/receptor complex LGI1 and ADAM22 regulate synaptic transmission. Science 313:1792–1795.

Gao Y, Hisey E, Bradshaw TW, Erata E, Brown WE, Courtland JL, Uezu A, Xiang Y, Diao Y, Soderling SH (2019) Plug-and-play protein modification using homology-independent universal genome engineering. Neuron 103:583–597.e588.

Good MC, Zalatan JG, Lim WA (2011) Scaffold proteins: hubs for controlling the flow of cellular information. Science 332:680–686.

Houge G, Rasmussen IH, Hovland R (2012) Loss-of-function CNKSR2 mutation is a likely cause of non-syndromic X-linked intellectual disability. Mol Syndromol 2:60–63.

Hu H, Haas SA, Chelly J, Van Esch H, Raynaud M, de Brouwer AP, Weinert S, Froyen G, Frints SG, Laumonnier F, Zemojtel T, Love MI, Richard H, Emde AK, Bienek M, Jensen C, Hambrock M, Fischer U, Langnick C, Feldkamp M, et al. (2016) X-exome sequencing of 405 unresolved families identifies seven novel intellectual disability genes. Mol Psychiatry 21:133–148.

Iida J, Nishimura W, Yao I, Hata Y (2002) Synaptic localization of membrane-associated guanylate kinase-interacting protein mediated by the pleckstrin homology domain. Eur J Neurosci 15:1493–1498.

Ippolito DM, Eroglu C (2010) Quantifying synapses: an immunocytochemistry-based assay to quantify synapse number. J Vis Exp 45:2270.

Kagan A, Melman YF, Krumerman A, McDonald TV (2002) 14-3-3 amplifies and prolongs adrenergic stimulation of HERG K^+ channel activity. EMBO J 21:1889–1898.

Kalachikov S, Evgrafov O, Ross B, Winawer M, Barker-Cummings C, Martinelli Boneschi F, Choi C, Morozov P, Das K, Teplitskaya E, Yu A, Cayanis E, Penchaszadeh G, Kottmann AH, Pedley TA, Hauser WA, Ottman R, Gilliam TC (2002) Mutations in LGI1 cause autosomal-dominant partial epilepsy with auditory features. Nat Genet 30:335–341.

Kim IH, Racz B, Wang H, Burianek L, Weinberg R, Yasuda R, Wetsel WC, Soderling SH (2013) Disruption of Arp2/3 results in asymmetric structural plasticity of dendritic spines and progressive synaptic and behavioral abnormalities. J Neurosci 33:6081–6092.

Lanigan TM, Liu A, Huang YZ, Mei L, Margolis B, Guan KL (2003) Human homologue of *Drosophila* CNK interacts with Ras effector proteins Raf and Rlf. FASEB J 17:2048–2060.

Lee JY, Lee LJ, Fan CC, Chang HC, Shih HA, Min MY, Chang MS (2017) Important roles of Vilse in dendritic architecture and synaptic plasticity. Sci Rep 7:45646.

Lein ES, Hawrylycz MJ, Ao N, Ayres M, Bensinger A, Bernard A, Boe AF, Boguski MS, Brockway KS, Byrnes EJ, Chen L, Chen L, Chen TM, Chin MC, Chong J, Crook BE, Czaplinska A, Dang CN, Datta S, Dee NR, et al. (2007) Genome-wide atlas of gene expression in the adult mouse brain. Nature 445:168–176.

Lesca G, Rudolf G, Bruneau N, Lozovaya N, Labalme A, Boutry-Kryza N, Salmi M, Tsintsadze T, Addis L, Motte J, Wright S, Tsintsadze V, Michel A, Doummar D, Lascelles K, Strug L, Waters P, de Bellescize J, Vrielynck P, de Saint Martin A, et al. (2013) GRIN2A mutations in acquired epileptic aphasia and related childhood focal epilepsies and encephalopathies with speech and language dysfunction. Nat Genet 45:1061–1066.

Lim J, Ritt DA, Zhou M, Morrison DK (2014) The CNK2 scaffold interacts with vilse and modulates Rac cycling during spine morphogenesis in hippocampal neurons. Curr Biol 24:786–792.

Lu C, Chen Q, Zhou T, Bozic D, Fu Z, Pan JQ, Feng G (2016) Micro-electrode array recordings reveal reductions in both excitation and inhibition in cultured cortical neuron networks lacking Shank3. Mol Psychiatry 21:159–168.

Mahrt EJ, Perkel DJ, Tong L, Rubel EW, Portfors CV (2013) Engineered deafness reveals that mouse courtship vocalizations do not require auditory experience. J Neurosci 33:5573–5583.

Nickels K, Wirrell E (2008) Electrical status epilepticus in sleep. Semin Pediatr Neurol 15:50–60.

Niday Z, Tzingounis AV (2018) Potassium channel gain of function in epilepsy: an unresolved paradox. Neuroscientist 24:368–380.

Nieder A, Mooney R (2020) The neurobiology of innate, volitional and learned vocalizations in mammals and birds. Philos Trans R Soc Lond B Biol Sci 375:20190054.

Nowak FV (2018) Porf-2 = Arhgap39 = Vilse: a pivotal role in neurodevelopment, learning and memory. eNeuro 5:ENEURO.0082-18.2018.

Owuor K, Harel NY, Englot DJ, Hisama F, Blumenfeld H, Strittmatter SM (2009) LGI1-associated epilepsy through altered ADAM23-dependent neuronal morphology. Mol Cell Neurosci 42:448–457.

Peltola MA, Kuja-Panula J, Liuhanen J, Voikar V, Piepponen P, Hiekkalinna T, Taira T, Lauri SE, Suvisaari J, Kulesskaya N, Paunio T, Rauvala H (2016) AMIGO-Kv2.1 potassium channel complex is associated with schizophrenia-related phenotypes. Schizophr Bull 42:191–201.

Polla DL, Saunders HR, de Vries BB, van Bokhoven H, de Brouwer AP (2019) A de novo variant in the X-linked gene CNKSR2 is associated with seizures and mild intellectual disability in a female patient. Mol Genet Genomic Med 7:e00861.

Purtell H, Dhamne SC, Gurnani S, Bainbridge E, Modi ME, Lammers SH, Super CE, Hameed MQ, Johnson EL 3rd, Sahin M, Rotenberg A (2018) Electrographic spikes are common in wildtype mice. Epilepsy Behav 89:94–98.

Rachalski A, Authier S, Bassett L, Pouliot M, Tremblay G, Mongrain V (2014) Sleep electroencephalographic characteristics of the Cynomolgus monkey measured by telemetry. J Sleep Res 23:619–627.

Rakhade SN, Jensen FE (2009) Epileptogenesis in the immature brain: emerging mechanisms. Nat Rev Neurol 5:380–391.

Rodriguiz RM, Colvin JS, Wetsel WC (2011) Neurophenotyping genetically modified mice for social behavior. Methods Mol Biol 768:343–363.

Rubenstein JL, Merzenich MM (2003) Model of autism: increased ratio of excitation/inhibition in key neural systems. Genes Brain Behav 2:255–267.

Salmi M, Del Gallo F, Minlebaev M, Zakharov A, Pauly V, Perron P, Pons-Bennaceur A, Corby-Pellegrino S, Aniksztejn L, Lenck-Santini PP, Epsztein J, Khazipov R, Burnashev N, Bertini G, Szepetowski P (2019) Impaired vocal communication, sleep-related discharges, and transient alteration of slow-wave sleep in developing mice lacking the GluN2A subunit of N-methyl-D-aspartate receptors. Epilepsia 60:1424–1437.

Schwenk F, Baron U, Rajewsky K (1995) A cre-transgenic mouse strain for the ubiquitous deletion of loxP-flanked gene segments including deletion in germ cells. Nucleic Acids Res 23:5080–5081.

Seppala EH, Jokinen TS, Fukata M, Fukata Y, Webster MT, Karlsson EK, Kilpinen SK, Steffen F, Dietschi E, Leeb T, Eklund R, Zhao X, Rilstone JJ,

Lindblad-Toh K, Minassian BA, Lohi H (2011) LGI2 truncation causes a remitting focal epilepsy in dogs. PLoS Genet 7:e1002194.

Soltani S, Chauvette S, Bukhtiyarova O, Lina JM, Dube J, Seigneur J, Carrier J, Timofeev I (2019) Sleep-wake cycle in young and older mice. Front Syst Neurosci 13:51.

Sun Y, Liu YD, Xu ZF, Kong QX, Wang YL (2018) CNKSR2 mutation causes the X-linked epilepsy-aphasia syndrome: a case report and review of literature. World J Clin Cases 6:570–576.

Syrbe S, Hedrich UB, Riesch E, Djémié T, Müller S, Møller RS, Maher B, Hernandez-Hernandez L, Synofzik M, Caglayan HS, Arslan M, Serratosa JM, Nothnagel M, May P, Krause R, Löffler H, Detert K, Dorn T, Vogt H, Krämer G, et al. (2015) De novo loss- or gain-of-function mutations in KCNA2 cause epileptic encephalopathy. Nat Genet 47:393–399.

Tassinari CA, Rubboli G, Volpi L, Meletti S, d'Orsi G, Franca M, Sabetta AR, Riguzzi P, Gardella E, Zaniboni A, Michelucci R (2000) Encephalopathy with electrical status epilepticus during slow sleep or ESES syndrome including the acquired aphasia. Clin Neurophysiol 111:S94–S102.

Therrien M, Wong AM, Rubin GM (1998) CNK, a RAF-binding multidomain protein required for RAS signaling. Cell 95:343–353.

Tsai MH, Vears DF, Turner SJ, Smith RL, Berkovic SF, Sadleir LG, Scheffer IE (2013) Clinical genetic study of the epilepsy-aphasia spectrum. Epilepsia 54:280–287.

Uezu A, Kanak DJ, Bradshaw TW, Soderblom EJ, Catavero CM, Burette AC, Weinberg RJ, Soderling SH (2016) Identification of an elaborate complex mediating postsynaptic inhibition. Science 353:1123–1129.

Vaags AK, Bowdin S, Smith ML, Gilbert-Dussardier B, Brocke-Holmefjord KS, Sinopoli K, Gilles C, Haaland TB, Vincent-Delorme C, Lagrue E, Harbuz R, Walker S, Marshall CR, Houge G, Kalscheuer VM, Scherer SW, Minassian BA (2014) Absent CNKSR2 causes seizures and intellectual, attention, and language deficits. Ann Neurol 76:758–764.

Viswanathan S, Williams ME, Bloss EB, Stasevich TJ, Speer CM, Nern A, Pfeiffer BD, Hooks BM, Li WP, English BP, Tian T, Henry GL, Macklin JJ, Patel R, Gerfen CR, Zhuang X, Wang Y, Rubin GM, Looger LL (2015) High-performance probes for light and electron microscopy. Nat Methods 12:568–576.

Wang X, Bey AL, Katz BM, Badea A, Kim N, David LK, Duffney LJ, Kumar S, Mague SD, Hulbert SW, Dutta N, Hayrapetyan V, Yu C, Gaidis E, Zhao S, Ding JD, Xu Q, Chung L, Rodriguiz RM, Wang F, et al. (2016) Altered mGluR5-Homer scaffolds and corticostriatal connectivity in a Shank3 complete knockout model of autism. Nat Commun 7:11459.

Wang F, Flanagan J, Su N, Wang LC, Bui S, Nielson A, Wu X, Vo HT, Ma XJ, Luo Y (2012) RNAscope: a novel in situ RNA analysis platform for formalin-fixed, paraffin-embedded tissues. J Mol Diagn 14:22–29.

Yang X, Qian P, Xu X, Liu X, Wu X, Zhang Y, Yang Z (2018) GRIN2A mutations in epilepsy-aphasia spectrum disorders. Brain Dev 40:205–210.

Yizhar O, Fenno LE, Prigge M, Schneider F, Davidson TJ, O'Shea DJ, Sohal VS, Goshen I, Finkelstein J, Paz JT, Stehfest K, Fudim R, Ramakrishnan C, Huguenard JR, Hegemann P, Deisseroth K (2011) Neocortical excitation/inhibition balance in information processing and social dysfunction. Nature 477:171–178.

Zagha E, Ozaita A, Chang SY, Nadal MS, Lin U, Saganich MJ, McCormack T, Akinsanya KO, Qi SY, Rudy B (2005) DPP10 modulates Kv4-mediated A-type potassium channels. J Biol Chem 280:18853–18861.

Zeisel A, Munoz-Manchado AB, Codeluppi S, Lonnerberg P, La Manno G, Jureus A, Marques S, Munguba H, He L, Betsholtz C, Rolny C, Castelo-Branco G, Hjerling-Leffler J, Linnarsson S (2015) Brain structure: cell types in the mouse cortex and hippocampus revealed by single-cell RNA-seq. Science 347:1138–1142.

Zhang Y, Chen K, Sloan SA, Bennett ML, Scholze AR, O'Keeffe S, Phatnani HP, Guarnieri P, Caneda C, Ruderisch N, Deng S, Liddelow SA, Zhang C, Daneman R, Maniatis T, Barres BA, Wu JQ (2014) An RNA-sequencing transcriptome and splicing database of glia, neurons, and vascular cells of the cerebral cortex. J Neurosci 34:11929–11947.

Zieger HL, Kunde SA, Rademacher N, Schmerl B, Shoichet SA (2020) Disease-associated synaptic scaffold protein CNK2 modulates PSD size and influences localisation of the regulatory kinase TNIK. Sci Rep 10:5709.